

A HARDWARE-ANYWHERE-IN-THE-LOOP SIMULATOR FOR
DYNAMIC REAL-TIME ANALYSIS OF ELECTRIC PROPULSION SYSTEMS

BY

MARCO JAKOB TAVERNINI

THESIS

Submitted in partial fulfillment of the requirements
for the degree of Master of Science in Electrical and Computer Engineering
in the Graduate College of the
University of Illinois at Urbana-Champaign, 2009

Urbana, Illinois

Adviser:

Professor Philip T. Krein

ABSTRACT

This work introduces a low-level real-time vehicle simulator with hardware-anywhere-in-the-loop (HAIL) capability. Vehicle dynamics are simulated on a high-performance workstation running a real-time operating system. The vehicle's battery pack is both modeled in simulation and interfaced externally, providing the option of establishing a baseline performance in the simulation, and then evaluating candidate battery packs against these results. This simulation test bed is applied to an electric vehicle and an unmanned underwater vehicle, two vehicle types that present very different loads to the batteries. The HAIL platform is validated against the verified simulated performance of both vehicle models, achieving an error of less than 2% across 25 trials. This paves the way for expansion to include an electric drive and dynamometer, as well as peripheral power electronics systems.

to my grandfathers

i has gschafft

ACKNOWLEDGMENTS

This work was supported in part by the Grainger Center for Electric Machinery and Electromechanics, and the Office of Naval Research.

I would like to extend my thanks to my thesis adviser, Dr. Philip T. Krein, for his support of my work. Without his insights and advice this project would never have made it this far.

A big thank you goes out to my parents as well, who have supported my ever-changing plans for what lies ahead with nothing but encouragement, support, and love.

And lastly, to the motley crew of Everitt Lab's finest, Alan, Eric, Frank, Andrew, and Andy. Wouldn't have made it this far without you guys. Now, to Murphy's!

TABLE OF CONTENTS

LIST OF FIGURES	vi
LIST OF TABLES	vii
1. INTRODUCTION.....	1
1.1 Project Motivation	1
1.2 Simulation Requirements.....	2
1.3 Literature Review.....	3
2. HARDWARE-ANYWHERE-IN-THE-LOOP.....	8
2.1 Hardware-Anywhere-In-The-Loop: HAIL	8
2.2 The Simulation.....	9
2.3 The Hardware Platform.....	10
2.4 Limitations and Possible Solutions.....	16
3. THE HYBRID ELECTRIC VEHICLE.....	19
3.1 The Hybrid Electric Vehicle	19
3.2 HAIL Performance Verification	23
4. THE UNMANNED UNDERWATER VEHICLE	27
4.1 The UUV Model	27
4.2 Simulation Results	33
4.3 Experimental UUV HAIL Results	36
4.3.1 Light-weight vehicle, 3 knots, 12 hours.....	36
4.3.2 Light-weight vehicle, 5 knots, 6 hours.....	39
4.3.3 Man-portable vehicle, 3 knots, 12 hours.....	42
4.3.4 Man-portable vehicle, 5 knots, 6 hours.....	45
5. CONCLUSIONS	49
6. FUTURE WORK.....	50
REFERENCES.....	52
APPENDIX A. UUV INITIALIZATION CODE.....	55
A.1 UUV Initialization Code, Light-Weight Vehicle.....	55
A.2 UUV Initialization Code, Man-Portable Vehicle.....	58
APPENDIX B. VEHICLE TRIAL DATA.....	61
B.1 Light Weight Vehicle Trial Data.....	61
B.2 Man Portable Vehicle Trial Data	63

LIST OF FIGURES

Figure 2.1: Analog input raw data	12
Figure 2.2: Current command with unfiltered voltage.....	13
Figure 2.3: Median filter	13
Figure 2.4: Filtered analog input.....	14
Figure 2.5: Current command with filtered voltage.....	14
Figure 2.6: Thermal protection circuit	15
Figure 2.7: Architecture of the hardware-anywhere-in-the-loop simulation	16
 Figure 3.1: Top-level view of the hybrid electric vehicle dynamic simulator.....	20
Figure 3.2: View of the lithium ion battery subsystem.....	21
Figure 3.3: View of the traction subsystem	22
Figure 3.4: Original GPIB-based HAIL response to dynamic current commands [22]	24
Figure 3.5: Analog control based HAIL performance	25
 Figure 4.1: Top-level view of the unmanned underwater vehicle dynamic simulator	27
Figure 4.2: UUV propulsion system	29
Figure 4.3: Vehicle dynamics	31
Figure 4.4: Torque output vs. shaft speed for propeller.....	32
Figure 4.5: Total vehicle power consumption during startup of 3-knot 12-hour LWV trial	37
Figure 4.6: Waveform of current withdrawn from pack during 3-knot 12-hour LWV trial.....	38
Figure 4.7: Close-up view of voltage waveforms during 3-knot 12-hour LWV trial.....	39
Figure 4.8: Close-up view of current waveforms during a 5-knot 6-hour LWV trial	40
Figure 4.9: Close-up view of voltage waveforms during a 5-knot 6-hour LWV trial	41
Figure 4.10: Close-up view of current waveforms during a 3-knot 12-hour MP trial.....	43
Figure 4.11: Complete view of voltage waveforms during a 3-knot 12-hour MP trial	44
Figure 4.12: Close-up view of power waveforms during a 3-knot 12-hour MP trial	45
Figure 4.13: Close-up view of current waveforms during entire 5-knot 6-hour MP trial	46
Figure 4.14: Close-up view of power waveforms during entire 5-knot 6-hour MP trial.....	47
Figure 4.15: Complete view of voltage waveforms during entire 5-knot 6-hour MP trial	48

LIST OF TABLES

Table 3.1: Overview of hybrid electric vehicle parameters	23
Table 3.2: Charge withdrawn using GPIB control.....	26
Table 3.3: Charge withdrawn using analog control	26
Table 4.1: Overview of parameters for both UUV models.....	33
Table 4.2: 5-knot endurance runs.....	35
Table 4.3: 3-knot 12-hour runs	35
Table 4.4: Energy consumed and errors observed for 3-knot LWV runs	37
Table 4.5: Energy consumed and errors observed for 5-knot LWV runs	41
Table 4.6: Energy consumed and errors observed for 3-knot MP runs	42
Table 4.7: Energy consumed and errors observed for 5-knot MP runs	46

1. INTRODUCTION

1.1 Project Motivation

An important consideration when designing a new electric propulsion system is the choice of battery pack and motor drive, and the effect of these choices on how the vehicle needs to be shaped and equipped to meet various goals established at the project onset. Finding a means to quickly evaluate different motor-drive and battery-pack configurations is crucial, and knowing the interactions between these two critical components provides insight into a prospective design with a given set of performance goals, whether they be vehicle range on a single charge, battery life time, or some combination of maximum output drive power for a given battery pack size.

Consider the behavior of a vehicle during rapid acceleration. The large power demands during acceleration will increase currents in a manner dependent on motor resistive drops, flux settings, inverter drops, battery state of charge (SOC), and other losses in the vehicle. This in turn decreases the available bus voltage. The inverter will react dynamically to deliver the requested power, further increasing the current and system losses. These dynamic interaction effects have profound design implications, as thermal hot spots and peak battery stresses tend to occur during fast dynamic interactions. In addition, the vehicle specifications that determine the load torque which the drive system must endure in order to reach a commanded vehicular speed can be adjusted as well. This opens the door to simple analysis of the impact of increased air resistance on the battery discharge time and resulting overall battery life.

Another application that requires a careful evaluation of the propulsion system is an unmanned underwater vehicle (UUV). These autonomous submersibles must perform a specific mission

for an extended period of time. The mission may be as simple as passive sonar observation, or may involve a patrol through hostile waters with an active electronic countermeasures package and frequent course corrections to avoid obstacles such as ships or mines. The proper sizing of the electrical storage system is essential; it must be large enough to successfully carry out the prescribed mission and be as small and efficient as possible.

In both the hybrid electric vehicle and the underwater vehicle cases, a fast and accurate simulation of the entire system would greatly improve the design process. The ability to pick and chose any component of the simulation, and replace it with an interface to real hardware, increases the benefits ten-fold, as now the candidate hardware for a particular design can be evaluated in a controlled laboratory environment. This architecture, in essence an expansion on the classic hardware-in-the-loop (HIL) design involving simulated plants and physical controllers, becomes a hardware-anywhere-in-the-loop (HAIL) platform.

1.2 Simulation Requirements

In order to successfully evaluate hardware in a bench-top simulation environment, the environment must achieve several disparate and critical goals. Most importantly, the original model that will form the basis of the HAIL simulator must be experimentally verified so that conditions being tested match real world observations. It is then necessary to adapt the simulation to operate in a real time execution environment without compromising the achieved real-world behavior. When the simulator has met the required performance conditions, a suitable operating system platform is chosen to facilitate the high performance simulation

operation, and allow for the program to interface with outside components. This requires driver support for such interfaces as GPIB and RS-232, digital-to-analog and analog-to-digital interface cards, and the computing platform itself. With the simulation capable of real-time execution and the appropriate hardware chosen and evaluated to ensure sufficient performance, the process of augmenting the simulation to incorporate real-world data input can begin.

The first component to be verified experimentally in this project is the energy storage subsystem. It provides both a relatively simple interface that minimizes the potential for technical issues, and a means of confirming the value of such a hardware/simulation platform. Once the fundamental operation capability of the platform is established using an existing lithium ion battery model and a developed battery interface, the bench-top platform can assume its full role as a HAIL system and can be shaped to suit the needs of the research and design process.

1.3 Literature Review

This HAIL platform, an extension of the HIL system, is not the usual route to implement a design tool. Usually, the device under test is a controller. The simulation stimulates the device and responds to its outputs, allowing for thorough evaluation of the controller behavior controlled conditions. Recently, researchers have moved to a more versatile platform to investigate other aspects of a complex electromechanical system. Implementation can involve only a motor drive and battery pack [1], or the entire vehicle can be interfaced with a simulation system to analyze the complete system [2].

The drawback of dynamic simulation is its complexity and extended run time. Ideally, a vehicle evaluation would involve both a fast high-level tool, such as the National Renewable Energy Lab's ADVISOR program [3], for long-term analysis and for lifetime fuel economy and cost issues, and a low-level tool for evaluation of stresses and design requirements. The high-level ADVISOR tool uses static performance maps to evaluate vehicle performance based on the steady-state behavior of vehicle subsystems. This approach is extremely useful for extended drive-cycle evaluation of basic energy performance in a vehicle system, and ADVISOR has become the de facto standard for many HEV analysis studies. The ADVISOR simulation works well as a means of investigating the relative performance of two designs [4], and the simulator itself has been validated with other static simulations of the components of a hybrid power train [5].

In [6] validation of complex models in a particular vehicle system is investigated. HIL is used to verify model operation in relation to the actual system. Several different simulation architectures are discussed, covering the entire spectrum of possible simulation environments and computational power needed to achieve a real-time HIL simulation. The most complex simulator discussed has a visual simulation component, which creates a virtual image of the vehicle on the screen and allows for direct user interaction with the simulator during a run. The work presented here falls in the center of this spectrum, as the model is complex enough to warrant the dedicated use of a high performance simulation computer, but not so large as to require several computers acting in concert to achieve real-time operation.

In [7] HIL systems are applied to power electronics and electric drive systems. The term *Power-Hardware-in-the-Loop* is used to describe these simulators, as the HIL system is not

used for the evaluation of low power analog/digital systems. Instead it is integrated into a high power propulsion system. This is similar to the work that is presented here, however with one distinction: mechanical drive and electrical storage components are left in simulation, while controllers and power electronics are deployed in actual hardware and connected to the computer. The approach in the following pages follows the opposite path. Vehicle systems and controls are simulated, and the energy storage system is implemented in a reduced size. This difference arises due to the contrasting goals each system sets out to achieve. In the case of [7] and most of the other work in the literature [4],[5],[6], the controller's behavior is of interest, and the energy storage system is left simply as a simulated component in the larger system. In contrast, the objective of this work is to evaluate potential hardware for use in a vehicle.

On the UUV front, interesting work is taking place in simulations of the vehicle as well as its underwater environment, with the aim of creating a medium from which the complete vehicle design can be evaluated under a varying array of conditions [8]. This simulation environment is capable of modeling multiple UUVs in a fully programmable ocean environment, allowing for the evaluation of the hardware configurations of each, as well as the autonomous control algorithms. In addition, a graphical environment allows for direct supervision of the vessel during its test, interaction with the submersible, and, once the vehicle design is finalized and deployed, use as an operator training simulator to familiarize personnel with the craft operation.

The Naval Undersea Warfare Center has taken a different approach to the evaluation of its torpedoes and other classes of UUVs [9]. It built a testing chamber that contains the vehicle, submerged in water and fixed in place. The chamber walls are lined with an array of sonar emitters, projecting the simulated target's acoustic signature to the torpedo's sonar system. The

torpedo's propulsion system is active, and through monitoring of the thrust output and control surface movement, the trajectory of the torpedo can be tracked and incorporated into the simulation environment presented to the system under test.

Another approach to the complex problem of evaluating a UUV design involves designing a complete set of tools intended to carry the development process from the initial design of each component to the final evaluation of the complete vehicle in the real world [10]. The authors use pure simulations of the proposed design, HIL evaluations of the first hardware builds, hybrid simulations involving a real operating environment but still utilizing some simulated data at the input, and finally the evaluation of the complete design in the intended operating environment. [10] is closest to the work presented here.

It is important to note that although the area of HIL simulation has gained newfound attention recently, this research dates back to the 1970s. Kassakian et al. [11] proposed one of the earliest predecessors of HIL platforms, the *parity simulator*. This early attempt at combining live circuitry and simulations was effective. It used analog computation modules in place of actual hardware, and drove real hardware with the signals generated. Although results were correct, the method was never fully embraced by industry, as skepticism of models and simulated results in design was common in the 70s and through to the early 90s [12].

An important note about the early work in this field is that there was insufficient computation power to achieve real-time plant simulation. Thus, a compromise was required. Work done in [12] instead focused on creating a versatile, modular system that would allow for rapid evaluation of different control schemes involving dc-dc, ac-dc, dc-ac, and ac-ac converter topologies. The converter controller was programmed via computer, and the modular design of

the power stage allowed for rapid reconfiguration to suit the needs of the work being done; in effect, the work was an early attempt at HIL design. Whereas most HIL work today involves simulated plants and real-world controllers, the principles are the same, and the earlier result was limited only by the meager computational performance available at the time.

Repeated testing of potential designs in real-world conditions represents one of the most expensive parts of the vehicle design process. The goal of the work presented herein is to provide a HAIL platform that can effectively take the place of repetitive real-world evaluation of different design iterations, pushing this stage of evaluation to the last part of a design endeavor. Doing so should significantly shorten the total time spent in design and verification, as well as eliminate costs of multiple full-scale testing samples. The HAIL's ability to work with reduced scale components and interpret data to deliver results for a proposed design is a key benefit.

2. HARDWARE-ANYWHERE-IN-THE-LOOP

2.1 Hardware-Anywhere-In-The-Loop: HAIL

The hardware-anywhere-in-the-loop architecture aims to expand the existing HIL concept beyond controller behavior verification using a simulated plant. The HAIL simulation platform incorporates the entire system, both plant and controller, into a simulation environment, and executes it in real time. Once this performance metric is achieved, and compatible hardware interfaces are evaluated and established, the HAIL platform is ready for use in dynamic system performance analysis. Because the entire dynamic system is contained in the simulation, evaluating the performance of any single component or subsystem of the overall design is a matter of removing that portion from the overall model and replacing it with input and output ports that interface to the hardware to be evaluated. In effect, it is possible to evaluate the operation of everything from a single operational amplifier found on a controller card to the entire energy storage system as implemented in an electric propulsion system. Assuming the entire model achieves real-time performance levels, the limits on what can be removed from the model and replaced with hardware depend primarily on the interfacing options available on the simulation platform. The HAIL platform thus consists of two different systems that work in tandem: the software model itself, and hardware to bridge the connection between the model and the outside world.

2.2 The Simulation

This project advances work in [13], [14], [15]. The goal is to achieve real-time operation by decreasing computation time. The simulation from [15] serves as the basis for this work, and consists of a traction system and energy storage system, developed over 10 years. In [15] a new lithium ion battery model was developed. The next step proposed was experimental verification of the model with a hardware-in-the-loop system.

In order to reuse as much of the original simulation as possible, the propulsion system simulation uses The Mathworks' xPC Target real-time operating system [16], featuring complete support of Simulink, the modeling environment of the simulator. The drawback of this platform, however, was the supported hardware. The version of xPC used for this work requires very specific peripheral hardware in order to function correctly. The largest hurdle is the required use of a 10-year-old Ethernet controller chip in order to allow for communication with the system via TCP/IP. However, newer versions of xPC have expanded support for newer hardware, and migration to this newer standard is slated to occur in the near future, enabling the use of a larger variety of hardware.

The simulation was optimized for real-time execution by tweaking the code and increasing the processing power and numerical solver's time-step size. The processing power was increased by overclocking the computer's CPU. Although prolonged increases above rated speed are not recommended, this was a means to evaluate the potential solutions before investing in expensive workstation class hardware. Increasing the simulation step size resulted in the largest gains in performance. However, if special care is not taken when the performance of the larger

step size is assessed, instabilities may find their way into the simulation, rendering the platform and its results invalid.

The largest usable step size was 8 μs using Simulink's fixed-step Runge-Kutta solver. This combination of time-step size and numerical algorithm required more computational power than is available on a high-end desktop machine capable of running the xPC Target operating system. When still larger step sizes were attempted, the simulator became unstable; the solver could no longer track the sinusoidal current waveforms of the induction machine drive. The instabilities occurred in the current feedback loop which was crucial to the implemented field-oriented control algorithm using hysteresis switching based on the machine's actual and commanded currents. In order to mitigate the onset of computational breakdown of the numerical engine, transport delays were inserted into each of the three phase's current feedback paths. These transport delays gave the simulator enough headroom to allow for stable operation at 11 μs , which was just enough to allow for real-time execution without compromising the results.

2.3 The Hardware Platform

Once the simulator achieved a real-time performance level, augmenting the model with a hardware interface could begin. Using xPC-supported A/D, D/A, RS-232 and GPIB interface hardware, the simulation PC is connected to external equipment that interfaces it with a lithium ion battery pack. This interface to the battery consists of a Quanser Q8 HIL control board, a programmable dc load, and a dc power supply. Using this combination of hardware, the

simulation's calculated current loads are imparted to the batteries. During simulator startup the dc load is initialized to a constant current mode and then ordered to respond to current commands from its analog input port. The analog interface card in the xPC provides these analog control signals generated by the simulator and captures the voltage reading the dc load measures across the battery pack. As a scaled down battery pack is connected to the simulation, the respective current commands and returned voltage signals will also have to be scaled in order to achieve the correct loading on the five battery cells being in a series configuration. With the number of cells in a series combination, n , and the number of parallel sets m , the following two equations govern the relationship between the small pack and the larger simulated one:

$$I_{5\ cells}^* = \frac{I_{pack}^*}{m} \quad (2.1)$$

$$V_{pack} = \frac{n (V_{5\ cells})}{5} \quad (2.2)$$

The Quanser Q8 HIL control board acts as the bridge between the simulation and the battery hardware. The raw output from the A/D is shown in Figure 2.1, and the noise can be clearly seen in the large random spikes in voltage as well as in the relatively large band in which the voltage level floats.

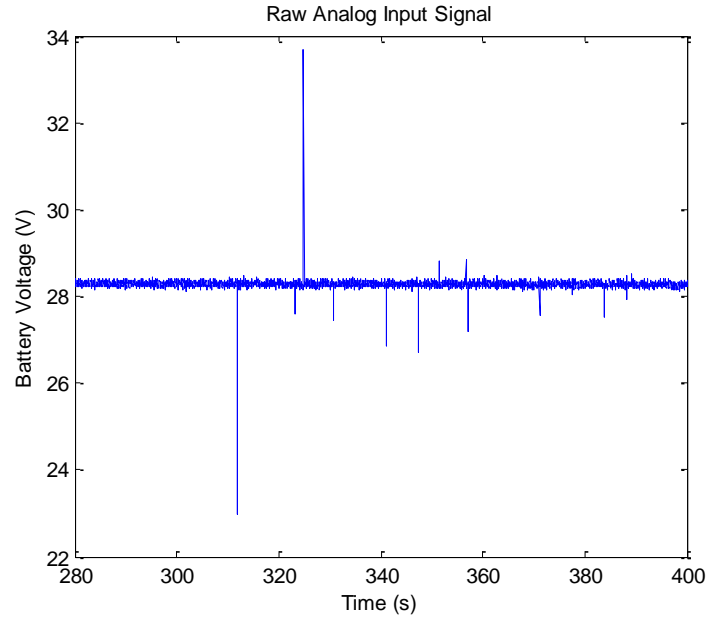


Figure 2.1: Analog input raw data

A rise in the voltage reading will correspond to a fall in the commanded current, and vice versa, as seen in Figure 2.2. The simulator attempts to maintain a commanded velocity profile, and thus control the power draw from the batteries. Figure 2.2 shows the current command for the attached pack, and the fluctuations in the current are apparent. In addition, the signal as a whole has substantial noise in it, and in order to reduce this the median filter is used as shown in Figure 2.3.

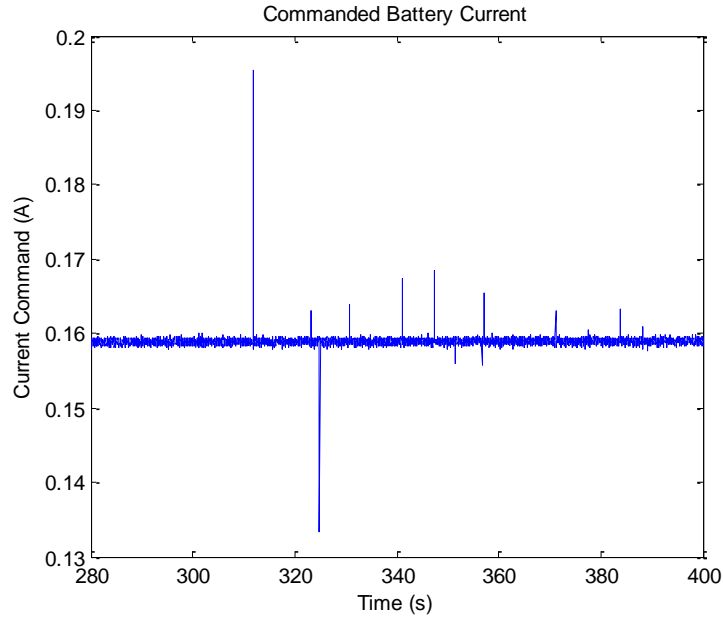


Figure 2.2: Current command with unfiltered voltage

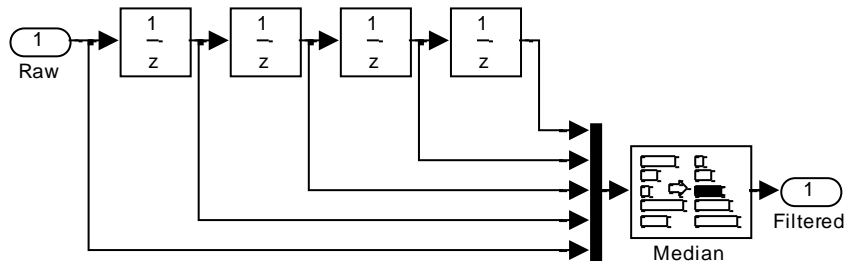


Figure 2.3: Median filter

As seen in Figure 2.4, the median filter has the desired effect on the voltage waveform; it eliminates the large spikes completely and reduces the ripple. As a result, the simulator's current command signal is flat, as seen in Figure 2.5. The net effect of this is a smoothing of the waveforms, producing a hardware-induced signal that closely resembles the simulated results.

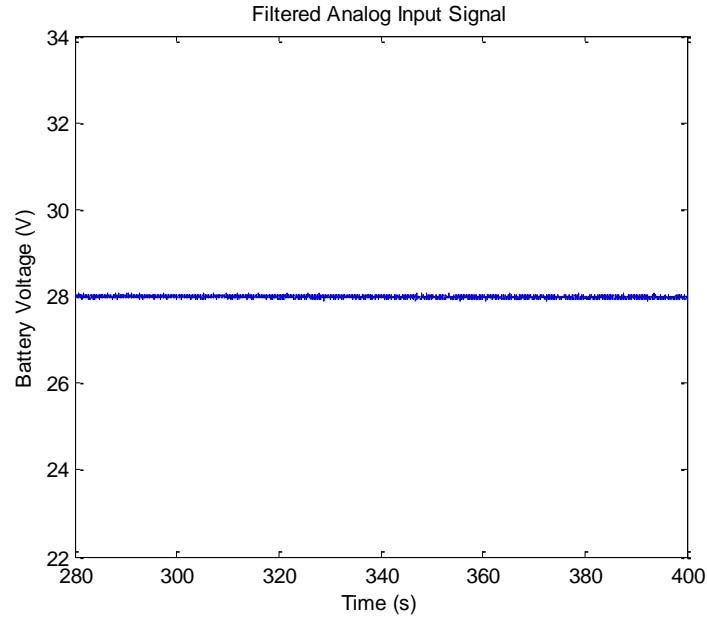


Figure 2.4: Filtered analog input

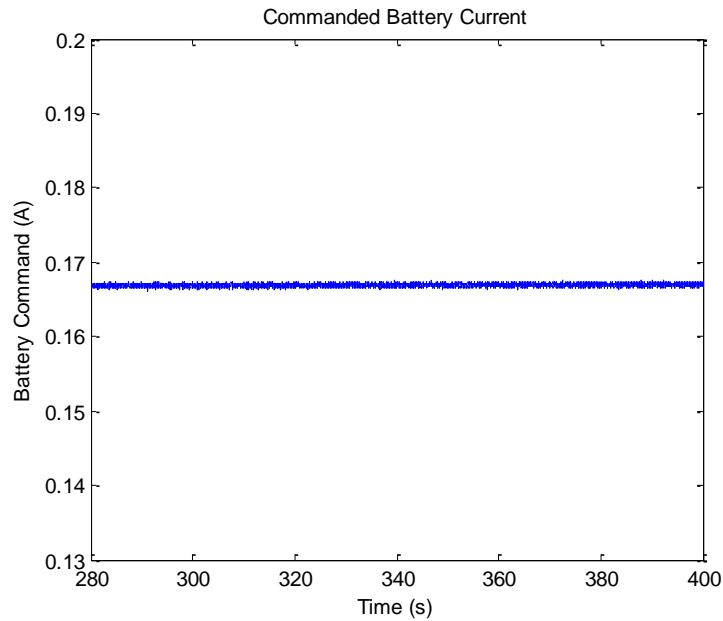


Figure 2.5: Current command with filtered voltage

In addition to acting as the interface between the simulation and the battery pack, the Q8 board possesses 32 digital I/O lines. One is used to implement a thermal protection circuit to safeguard against thermal runaway of the batteries during extended cycles. The schematic in

Figure 2.6 shows the circuit implemented in the HAIL simulation platform. The thermal sensor, a LM35 Precision Centigrade Temperature sensor, outputs a voltage that is linearly proportional to the temperature at the contact surface of the device. This output signal is then compared to a set point voltage representing the maximum allowable temperature, which, in the case of the lithium ion batteries used, is 45° C [17]. As long as the temperature remains below this maximum, the simulation continues uninterrupted. If the threshold temperature is surpassed, a breaker is triggered that severs the battery pack from the dc load and power supply, and a digital command line to the Q8 is pulled to ground, initiating a simulation shutdown.

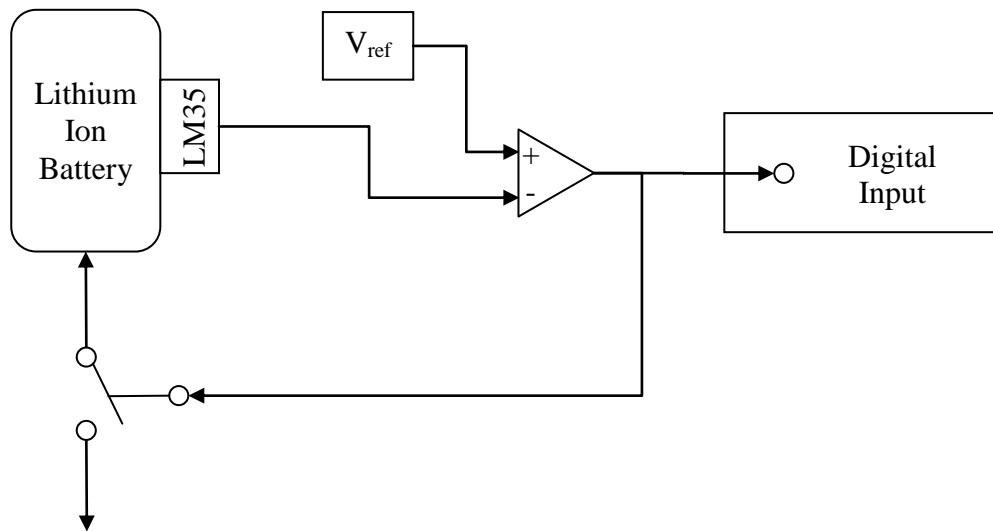


Figure 2.6: Thermal protection circuit

The simulator's internal data logging is verified by an external data acquisition unit (DAQ), controlled with a Labview program. The DAQ measures current flow through and voltage across the battery every two seconds, saving the data to the command computer for later data analysis and verification. Communication between the command and simulation computers

machine is achieved through a private TCP/IP network, which provides for direct control of the simulation and external network interference.

The entire hardware setup is shown in the top-level view in Figure 2.7 illustrating the key system components and the primary communications and power-flow paths. The thermal protection circuitry from Figure 2.6 is omitted from the diagram in order to provide a clear overview of the critical system components.

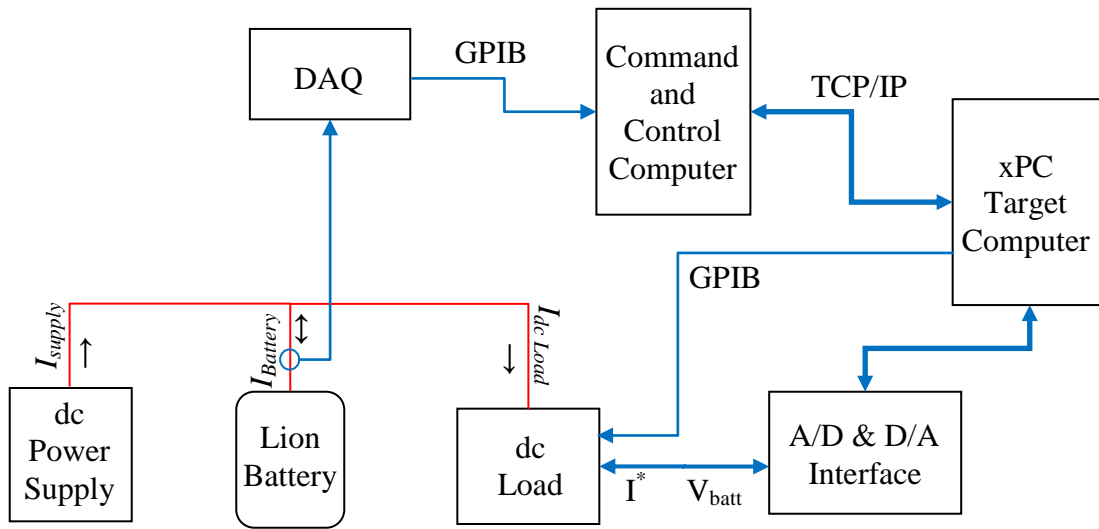


Figure 2.7: Architecture of the hardware-anywhere-in-the-loop simulation

2.4 Limitations and Possible Solutions

A few limitations of the HAIL platform were discovered during this research. Besides the restriction in the number of available analog and digital connections, the underlying platform software has its own set of limitations. To fully characterize the battery, both short and long

term models are required. The short term model is from [18]. In order to create a long term model, the HAIL platform would have to operate continuously for several months.

The simulator's inability to operate for such extended periods of time was discovered during the initial trials involving long term UUV simulations. The simulator had never been used for periods lasting more than 12 hours, and the endurance tests of the UUV would last for at least 35 hours. After a time span that varied from 13 to 15 hours, a numerical error appeared to cause a spike in the traction subsystem; the applied electrical torque dropped to near zero, and induced a regenerative energy recovery event. These events drove the load current into a high negative range. This initiated a battery recharge procedure that increased the battery's SOC above the maximum safe levels, triggering the safety algorithms and ending the simulation.

The most likely cause of the instability appears to be a combination of factors. The xPC operating system is based on a custom 32-bit real-time platform. Depending on the sample size and total execution time, this will become an issue. Assuming the xPC software keeps track of the number of time steps completed, the upper limit on the total is 2^{32} . The HAIL platform operates on a sample time of 11 μ s, meaning that approximately 90 909 time steps occur every second. This results in:

$$\frac{4,294,967,296}{90909.09} = 47244.64 \text{ seconds, maximum execution time}$$

$$\frac{47244.64 \text{ s}}{3600 \frac{\text{s}}{\text{hr}}} = 13.124 \text{ hours, maximum execution time}$$

This result conforms to the observed instability of the simulation that occurs shortly after 13 hours of run time. This cannot be a coincidence. Although it may not be the only cause of the

system instability, it is certainly a key issue preventing long-term execution. For comparison, if a 64-bit operating platform were available, the maximum time horizon at an $11\mu\text{s}$ step size would extend to over 97 million years, providing ample headroom for even the longest term hardware evaluations.

The same 32-bit limit observed in the xPC platform extends to MATLAB as well. As laid out in the MATLAB technical support pages [19], the 32-bit variant for MATLAB ran on a Windows XP platform with a maximum workspace size of ~ 1700 MB and a maximum matrix size of ~ 1189 MB. The number of elements is also restricted to $\sim 155^6$ for a real double array and $\sim 1246^6$ for a int8 array. If the move were made to a 64-bit version of MATLAB running on a 64-bit Windows platform, the limits essentially become those of the underlying platform itself. The maximum workspace and matrix sizes are constrained by the platform's maximum addressable memory, approximately 8 terabytes. The number of elements in either form of array is $2^{48}-1$, or approximately 2.8^{14} .

With 64-bit operation out of the question, a solution to this issue involves the creation of a supervisory program that monitors the state of the simulation, and at a preprogrammed time initiates a shutdown of the simulation. The last known state of the simulation is captured just before it ends and stored in the supervisor's program. Once stopped, the xPC platform reinitializes to the initial state of the loaded model. The supervisor can then overwrite the initial conditions with the set observed at the break. Once complete, the supervisor can restart the simulation, and the process can now repeat indefinitely, allowing for arbitrarily long trials. As the size of the data sets captured could be made to conform to the limits imposed on it by the software platform being used, the only constraint at this point would be available data storage.

3. THE HYBRID ELECTRIC VEHICLE

3.1 The Hybrid Electric Vehicle

The first model applied to the HAIL platform is an HEV simulation. This reference system is a comprehensive dynamic model of a hybrid electric vehicle. The model incorporates various mechanical forces, including air drag, tire losses, transmission operation and drive train losses, as well as the complete electrical drive train power consumption and peripheral component energy needs. The propulsion system components are all based on dynamic models which not only provide steady-state power consumption information but also take into account device behavior during changes in operating conditions. The model has been extensively validated against real systems – from the original hybrid vehicle it was based on [13], to the lithium ion battery model derived in 2008 [18].

The top-level view of the HEV model can be seen in Figure 3.1. Storage and propulsion systems are separated into two large subsystems, with the peripheral energy consumption and power calculations found alongside. Data of interest are saved to the local machine workspace running the simulations. When the simulations are implemented on the xPC platform for high-speed executions and real-time runs, data is saved to the local disk in order to speed up execution time.

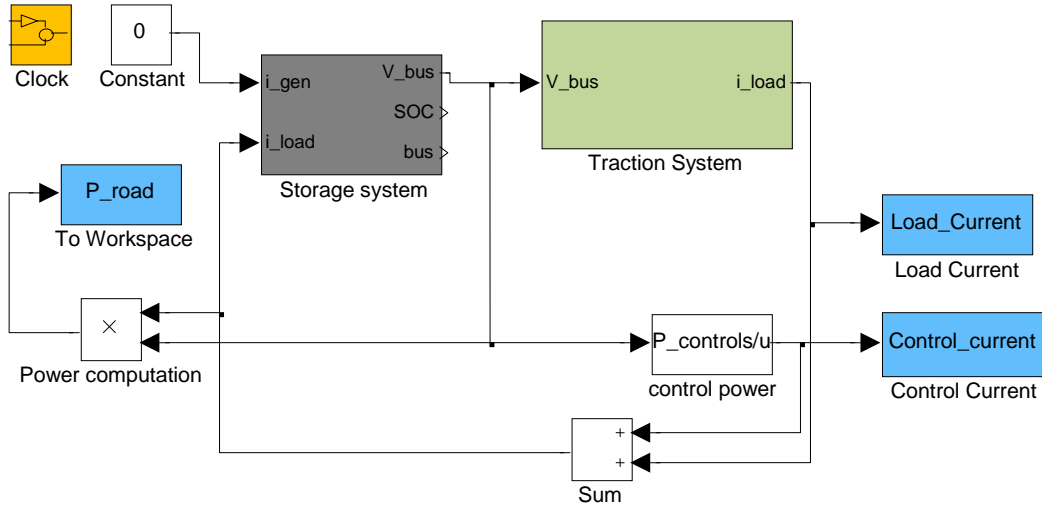


Figure 3.1: Top-level view of the hybrid electric vehicle dynamic simulator

The storage system block in Figure 3.1 contains the lithium ion battery model seen in Figure 3.2 with the input ports for both load and generation current and output ports for the SOC and terminal voltage. Generation current would come from an onboard power source such as an internal combustion engine or fuel cell. The battery model is a comprehensive simulation of a Panasonic CGR1850A lithium ion cell, as implemented by Kroeze in [18]. The model can track the SOC of the battery and, from this and the current load information, calculate the resulting terminal voltage and internal battery power losses incurred during use. Since all the relevant battery data represent the behavior of a single cell, the model includes relevant scaling factors to allow for series and parallel combinations of batteries to be modeled. This allows for simple reconfiguration of the battery pack by modifying only two parameters.

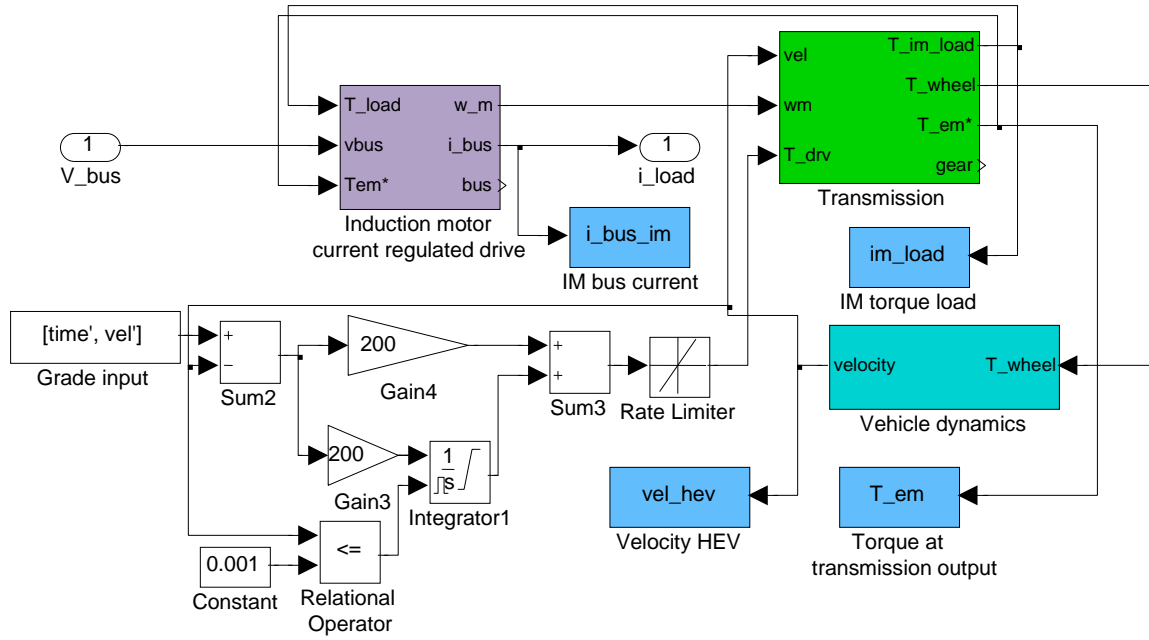


Figure 3.3: View of the traction subsystem

The vehicle profile used for the initial HAIL platform verification is based on two HEVs built at the University of Illinois in the mid 1990s. Detailed verification of the first complete HEV model was done using a Ford Escort platform [20]. The HEV simulation used in this work is a derivative of the original, refined to incorporate results of continued work with HEVs. The basic vehicle parameters seen in Table 3.1 have changed as well, and represent a generic hybrid vehicle that is consistent with today's designs. The vehicle uses a battery pack consisting of 23 parallel sets of 99 lithium ion battery cells, resulting in a nominal bus voltage of 366.3 V and total energy storage of 46 Ah. The power bus supported by the batteries is tied directly to the propulsion subsystem, meaning that with the changing battery voltage during a drive cycle the current draw will vary in order to maintain the commanded power output.

Table 3.1: Overview of hybrid electric vehicle parameters

Drag Coefficient, C_d	0.28
Frontal Area	2.0 m^2
# of Battery Cells	2277
Total Mass	1295 kg
Total Onboard Energy Storage	16.85 kWh

3.2 HAIL Performance Verification

The verification hardware was a scaled-down version of the simulated vehicle's onboard energy-storage system. A battery pack consisting of five Panasonic CGR1850 cells was run through five trials. The vehicle simulation used the FUDS/UDDS 1505 velocity profile [21], and the five sets of trial data were compared to the results obtained by the pure simulation. The adaptation of the HEV model to function on the HAIL platform was done in two stages, as detailed in [22]. The first attempt at HAIL platform integration took the form of a GPIB-controlled dc load receiving current commands and transmitting back voltage readings. This proved to be problematic, as the inherent delay of the GPIB interface had a deleterious effect on the results. Figure 3.4 shows the original result, with the commanded waveform and resulting battery voltage delayed significantly in relation to the simulated result. The most serious effect of this delayed response was the system inability to successfully track dynamic current shifts that occurred faster than the GPIB's response time, which was limited to 0.25 s by the protocol itself [23].

The transients present in the simulated curve are ignored by the HAIL simulation commands to the battery. The effect of the delay is clearly visible in the voltage plots, with a half-second

delay seen from the time the current command is issued until the battery pack response is transmitted back to the PC.

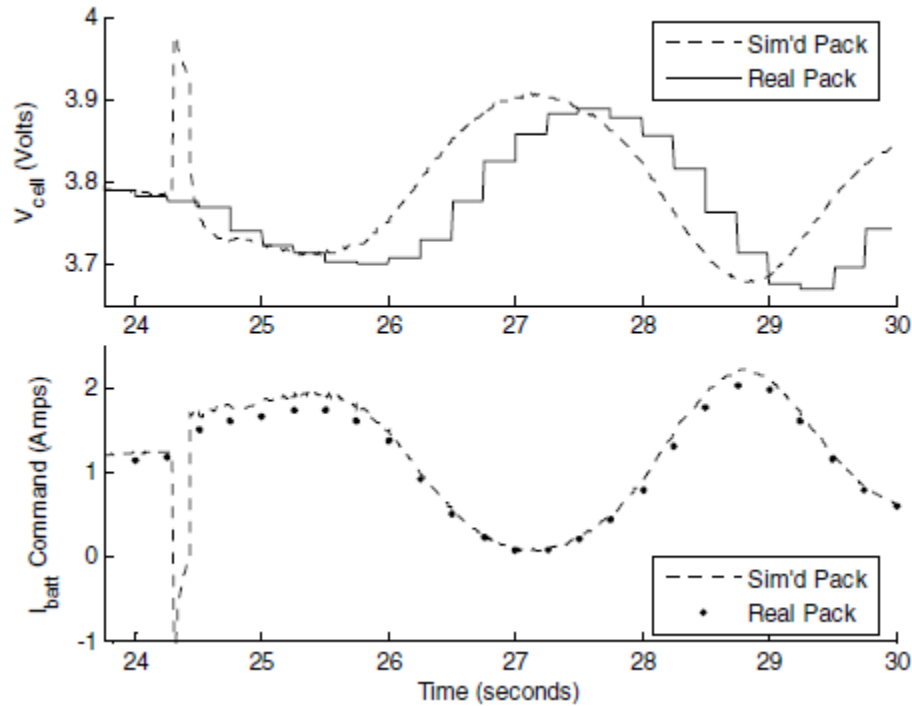


Figure 3.4: Original GPIB-based HAIL response to dynamic current commands [22]

The solution was to use the dc load's analog command capability, enabling much faster reaction time to commands by the dc load, and faster voltage read-back. Figure 3.5 shows the same time span as seen in Figure 3.4, except the dc load is now controlled by a 0-10 V analog output signal generated by the Quanser Q8 board. The dc load's battery voltage signal is captured by an analog-to-digital converter present on the board. The signal is then used by the simulation to perform calculations of consumed power and needed current.

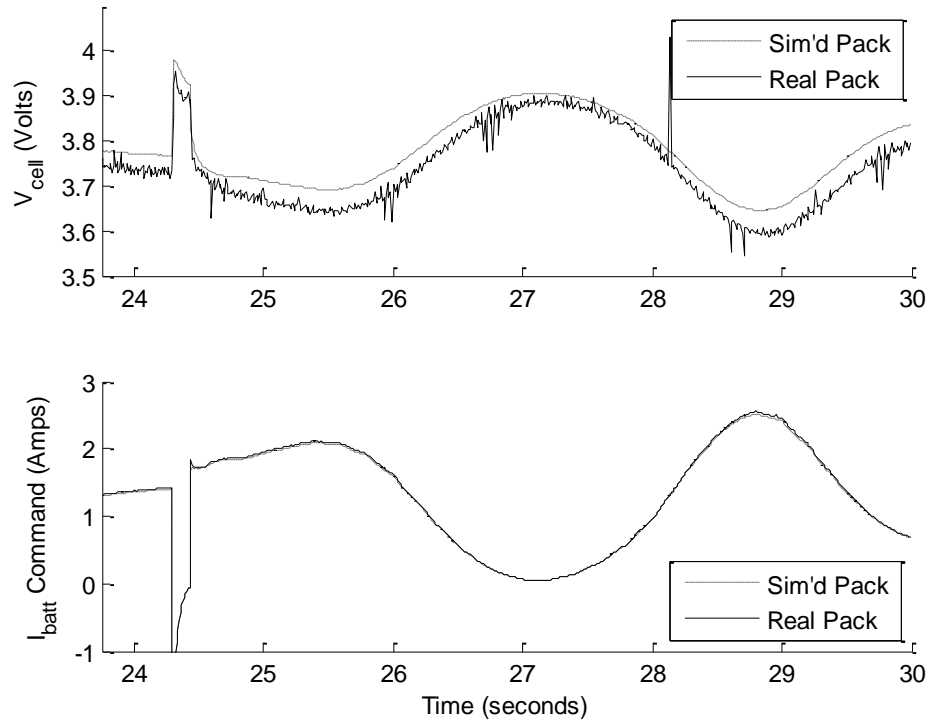


Figure 3.5: Analog control based HAIL performance

The effect of the skipped transients in the GPIB-based HAIL platform was an error in the measured charge withdrawn from the battery packs. Tables 3.2 and 3.3 list the results from the GPIB and analog designs, and the difference is clear. The GPIB pack falls 75 C short of the simulated amount withdrawn from the pack, a difference of 15.05%. An interesting byproduct of this large difference is the impact of high speed transients on the batteries. The missed transients that result from rapid acceleration and deceleration commands appear to account for a non-trivial portion of the cycling the battery is exposed to. Thus, the design of the battery and the energy storage system must take into account dynamic behaviors of the vehicle.

Table 3.2: Charge withdrawn using GPIB control

Battery	Charge Withdrawn
Real Pack	424.5 C
Simulated Pack	499.7 C

Table 3.3: Charge withdrawn using analog control

Battery	Charge Withdrawn
Real Pack	500.8 C
Simulated Pack	499.7 C

The analog HAIL platform duplicates the simulated performance nearly perfectly, with an error in charge withdrawn of only 0.22%. Such a small error highlights the accuracy of the HAIL platform operation, and illustrates its inherent value to any design team faced with a choice of battery chemistries and configurations. Furthermore, by extending or altering the hardware interfaced with the simulation, further aspects of the design can be evaluated. Examples are the traction subsystem or internal power distribution network. In addition to aiding the design effort of a new propulsion system, the HAIL platform could further validate the Kroeze battery model by providing the possibility of a 1:1 comparison of the real pack and model behavior.

4. THE UNMANNED UNDERWATER VEHICLE

4.1 The UUV Model

The HAIL system can be expanded to include other vehicle types. Figure 4.1 shows the adaptation of the HEV simulator used in Chapter 3. It incorporates the experimentally verified lithium ion battery model and an electric machine coupled to a propeller propulsion system coupled with a load intended to simulate the movement of a submarine through the water.

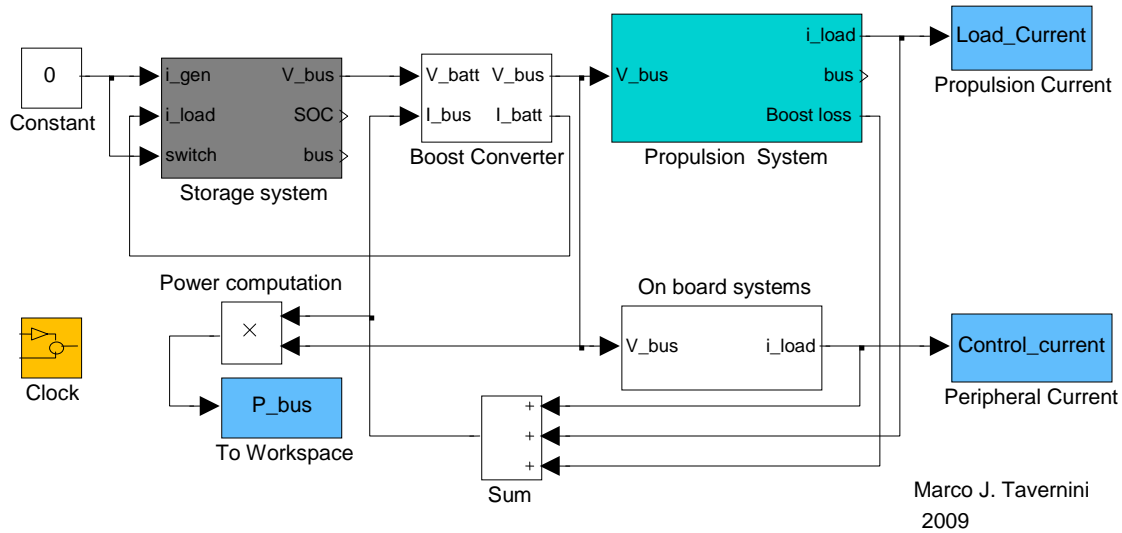


Figure 4.1: Top-level view of the unmanned underwater vehicle dynamic simulator

In order to meet the generally accepted 28 V military bus standard [24], the battery pack is configured to a seven-cell series, n parallel arrangement to provide a voltage that falls in the range of 21-28 V, and with an n set to provide sufficient storage to accomplish the required mission objectives. This battery voltage is then regulated to a stable 28 V by means of a boost converter. From there it is fed into the vehicle's power bus.

The propulsion system can be composed of any of numerous possible combinations involving different drive and energy storage technologies. The drive system can be a simple externally mounted propeller, as is common in most underwater vehicles, or it could consist of a more complex impeller system designed to both propel the craft forward and act as the steering mechanism for the ship. Moving through water will, by definition, incur a higher energy cost than moving through air due to the higher density of water, and this will need to be accounted for in the simulation. However, undersea craft move far slower when compared to their ground or air based counterparts. This trade-off in energy costs is resolved in the ship's favor. However, if the vehicle is to be put to sea for an extended period of time, a comprehensive means of energy storage, perhaps including energy harvesting, will be needed to complete the journey.

In this UUV simulation, the propulsion system is in the form of a permanent magnet synchronous machine (PMSM), also known as a brushless dc (BLDC) machine. The BLDC operates off a 168 V dc bus, requiring a two-stage voltage-boost conversion. The first stage boosts the voltage to 84 V, and the second brings this level up to the 168 V needed for proper operation. A hysteretic current-controlled inverter is used to drive the motor at the commanded vehicle speed. Figure 4.2 shows the propulsion subsystem layout, including the vehicle dynamics and boost converter power-loss calculation subsystems.

The BLDC modeled is a nonsalient machine, which implies that $L_q = L_d$. This reduces the torque equation (4.4) to the following:

$$T_e = \frac{3}{2} \frac{P}{2} (\lambda_m I_{qs}) \quad (4.5)$$

This equation can be rearranged to find the current needed to achieve a certain torque, enabling torque-controlled actuation of the BLDC. As the vehicle dynamics impart a torque load on the motor shaft, the speed command PI loop output can be taken to drive the machine torque command to the desired operating state in order to achieve a commanded velocity. The commanded I_{qs} current equation becomes:

$$I_{qs}^* = \frac{2}{3} \frac{2}{P} \frac{1}{\lambda_m} T_e^* \quad (4.6)$$

This result implies that the d-axis currents have no useful effect on motor operation. In order to minimize the losses incurred by these unnecessary currents, the commanded current is simply set to zero. This ensures that the hysteretic current controller will try to drive I_{ds} to zero, thus minimizing losses due to the d-axis winding [21].

The motor load is created by taking the input power and equating it to the necessary output power needed to drive the submarine at a given velocity, as seen in Figure 4.3. The power produced by the propeller is found using a look-up table that relates a given rotational speed to a load torque. Given this, the power generated by the propeller can be found (4.7). The power transfer between the propeller and the water is given an efficiency of 70%, in order to account for cavitation and other higher-order effects not modeled in this first-order approximation. Now

that the power transferred into the water is known, this value can be inserted into the velocity equation (4.8), and the resulting submarine speed can be ascertained.

$$P_{prop} = 0.7 \omega_r T_p \quad (4.7)$$

$$Velocity = \sqrt[3]{\frac{2 P_{prop}}{\rho C_d A_f}} \quad (4.8)$$

The coefficient of friction, C_d , is assumed to be ~ 0.3 . This number provides an approximation for the vehicle drag coefficient. Although the torpedo-like shape of the UUV should, on its own, yield a lower drag coefficient, protrusions from the hull, such as propeller and control pylons, detract from the optimum, yielding the approximation of 0.3. The frontal area, A_f , varies with the vehicle type being modeled, but in both cases the area is approximated to the cross-sectional area of the UUV's circular body. As the UUV's exact mechanical design is unknown, and the cross-sectional area of any control or support pylons would be minimal, they can be neglected without a noticeable impact on the result.

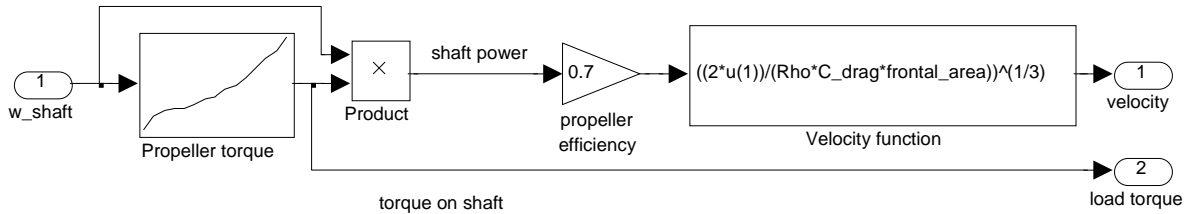


Figure 4.3: Vehicle dynamics

The propeller speed vs. torque output relationship is based on experimental data gathered and implemented in previous work [11]. Figure 4.4 shows the plot of this relationship. The original data was taken from a cooling fan torque load on an induction machine as its rotational speed increased. This data was modified slightly to better represent the propeller dynamics operating

in water. The x-axis of the plot was compressed by a factor of 10 in order to mimic real propeller behavior, which would generate substantial torque at much lower rotational speeds, given that the operating medium, water, has a density 1000 times greater than air.

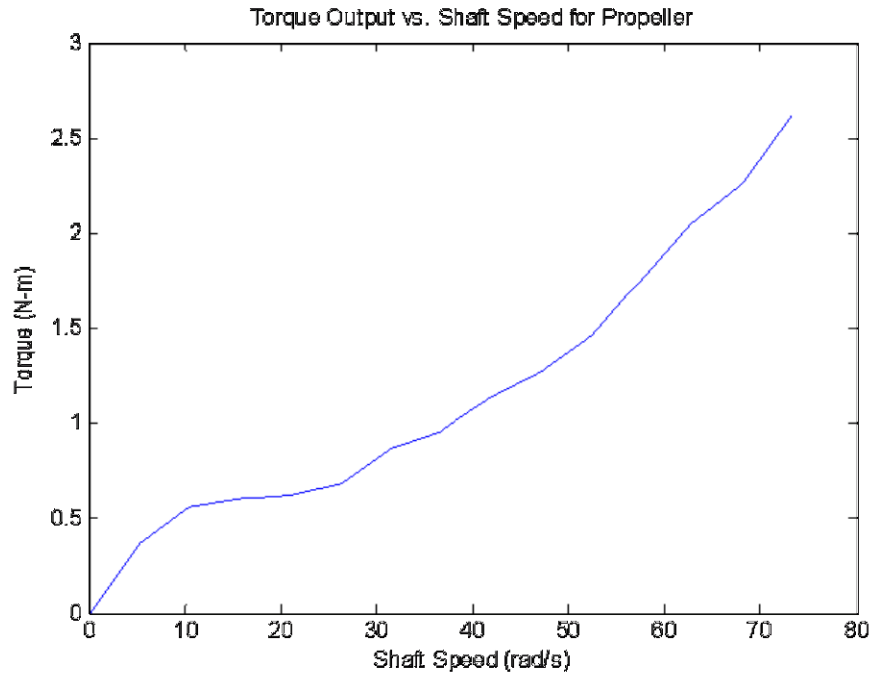


Figure 4.4: Torque output vs. shaft speed for propeller

A key requirement of the propulsion system will be a very high torque output at a low rotational speed, in order to create the power necessary to propel the submarine without inducing cavitation at the blades. To avoid shaft speeds in excess of 7000 RPM a gear box is required to reduce the propeller rotational speed. The gear box implemented in the UUV model imparts a 10:1 reduction of the BLDC's shaft speed to the propeller shaft.

In addition to the propulsion system, the model can accommodate additional auxiliary system loads such as active and passive sonar, payload delivery, GPS navigation, and communications. The current profile of each auxiliary load can be incorporated into the model and applied to the

electrical bus when activated. Incorporating these triggered subsystems into a set of simulation and HAIL trials is straightforward. First, the initialization file of the vehicle model is modified to implement current profiles of the relevant subsystems. Triggering these subsystems then becomes a matter of editing the activation profiles already embedded in the simulation. The profiles need to be altered to reflect the on-state behavior of a particular system. Once this is complete, the subsystems will start at the commanded times, and the changes in current will be imparted on the vehicle's electrical storage system.

Two different-sized vehicles are implemented and modeled in this simulation; one belongs to the man-portable class, the other to the light-weight vehicle class. Both are driven by the same BLDC propulsion system. The two designs differ primarily in their onboard energy-storage capacities and physical size. Further details of each vehicle class can be seen in Table 4.1 below, which lists some of the most important attributes.

Table 4.1: Overview of parameters for both UUV models

	Man Portable Vehicle	Light-Weight Vehicle
Drag Coefficient	0.3	0.3
Diameter	0.1905 m	0.3239 m
Frontal Area	0.0285 m ²	0.0823 m ²
Mass	45 kg	240 kg
# of Battery Cells	217	777
Onboard Energy	1.5 kWh	5.4 kWh
Endurance	35.7 hours @ 3 knots	53 hours @ 3 knots
Requirements	11.9 hours @ 5 knots	7.3 hours @ 5 knots

4.2 Simulation Results

Once the UUV vehicle classes have been defined, the performance of each vehicle must be evaluated in endurance tests. Each vehicle's speed is commanded to either 3 or 5 knots (1.54

m/s or 2.57 m/s respectively), and allowed to run until the battery pack reaches an SOC of 20%, at which point the system shuts down to prevent a deep discharge of the lithium ion cells. The propulsion system onboard each vehicle accounts for the majority of the power drain on the batteries. As a result, the endurance and range of these vehicles will be limited by the available storage capacity of each battery pack. The SOC window is limited to between 85% and 20%, meaning the vehicle has access to only 65% of the pack's total charge capacity. Another potential hurdle to system performance is the assumption that the propeller is only 70% effective in transferring shaft power to the surrounding environment. This results in an additional 42% mechanical power needed to drive the submarine to the desired speeds.

The effects of these assumptions and restrictions can be seen in Table 4.2, with the actual simulated times falling short of the prescribed goals. If the full 1.5 kWh of energy were available and the propeller assumed to be more efficient in power transfer, the goal would be within reach for each case. Unlike the man-portable vehicle, which appears to suffer greatly from the limited energy storage capacity and propeller losses, the light-weight vehicle comes to within an hour of the desired goal. This relatively good result can be attributed to the greatly reduced power-consumption numbers, which almost make up for the capacity limits and mechanical losses.

In particular, the power consumption of the light-weight vehicle falls well below the goal that was set. This can be attributed to the use of a gear box to reduce the rotational speed of the propeller instead of relying on a direct drive system, and the subsequent efficient operation of the motor at those speeds. Another potential error could arise from the fact that the vehicle dynamics being applied to the BLDC system are, indeed, only a first-order approximation of

the rather complex hydrodynamics of a submerged craft moving through water. This could, in part, account for a portion of the system's high performance level.

Table 4.2: 5-knot endurance runs

Vehicle	Duration of Run	Predicted Endurance Time	Average Power Consumption	Goal
LWV	6:20:18	7:20:00	379 W	800 W
Man-Portable	6:05:08	11:54:00	144.6 W	126 W

The inability to operate the simulator for extended periods of time became a hindrance when the long-term UUV tests were slated to be performed. However, in place of an endurance run, data was gathered for 12-hour mission runs at three knots, providing a reference for extrapolation of how long the vehicle battery packs would survive travelling at that speed.

Table 4.3: 3-knot 12-hour runs

Vehicle	SOC at end of 12 Hour Run	Predicted Endurance Time	Average Power Consumption	Goal
LWV	0.6308	35:35:02	97.99 W	102 W
Man-Portable	0.4921	21:47:38	47.42 W	42 W

As seen in Table 4.3, the LWV vehicle's predicted endurance time is well short of the mandated time, once again due to the 65% limit imposed on the available energy from the battery. However, as the average power consumption is below the mandated level, if all the energy were available, the vehicle would exceed the mandated time. In the case of the man-portable vehicle, the average power consumption is slightly above the goal, and the endurance time is again short of the mandate.

4.3 Experimental UUV HAIL Results

With the simulations of each set of vehicle configuration and mission duration and speed combinations complete, the same conditions must now be imposed on a scaled down battery pack. The results of these trials will serve to verify two things: first, that the battery model correctly mimics the real world behavior of the battery cells, and second, and perhaps more importantly, that the bench-top HAIL simulation system is a capable tool that can be successfully used to evaluate the performance of a component of a larger design in controlled laboratory conditions.

4.3.1 Light-weight vehicle, 3 knots, 12 hours

The first condition to be completed, a 3-knot 12-hour endurance run of the light-weight vehicle, yielded excellent results, as seen in Table 4.4. The second trial showed the best results, exhibiting a deviation between the DAQ data and simulated results of only 0.8495%. The only real issue encountered during these trials was the premature end of the data collection in trial 4, attributed to an uncontrolled Windows XP update and restart. Although the DAQ only recorded six hours of information, the error rate of the data obtained still fell within the range of the rest. The outlier of the 3-knot 12-hour LWV trials was the fifth, and upon closer examination of the data, it appears the current source's $\pm 4.5\%$ error range was the culprit [26], as the voltages measured by both the HAIL hardware and the DAQ were consistent. Of note also is the miniscule error seen between the HAIL platform's internally computed power consumption and the simulator's original numbers. This indicates that the HAIL platform, when supplied with the correct voltage readings at the battery pack, will, in fact, correctly track the power commands in order to achieve the prescribed velocity.

Table 4.4: Energy consumed and errors observed for 3-knot LWV runs

	HAIL Energy	DAQ Energy	Sim Energy	HAIL-DAQ Error	HAIL-Sim Error	DAQ-Sim Error
Trial 1	1167.8 W-hr	1146.3 W-hr	1167.7 W-hr	1.8409%	0.0074%	1.8337%
Trial 2	1167.7 W-hr	1157.8 W-hr	-	0.8517%	0.0023%	0.8495%
Trial 3	1167.7 W-hr	1148.5 W-hr	-	1.6408%	0.0003%	1.6406%
Trial 4*	563.48 W-hr	554.37 W-hr	563.52 W-hr	1.6233%	0.0078%	1.6155%
Trial 5	1167.7 W-hr	1130.9 W-hr	-	3.1526%	0.0002%	3.1525%
Mean				1.8219%	0.0036%	1.8184%

*Note: this trial's DAQ data collection ended prematurely due to PC restart

The startup of the vehicle and rampup to command velocity is seen in Figure 4.5. The HAIL and DAQ curves follow a similar path, exhibiting a more damped response to the increased power demand than that seen in the simulated case. Also, the delay seen between the DAQ and HAIL power plots can be attributed to the inability, at present, to synchronize the start of the external DAQ data capture with the HAIL startup. The two-second sampling period used by the DAQ also contributes to the slight misalignment between the two curves.

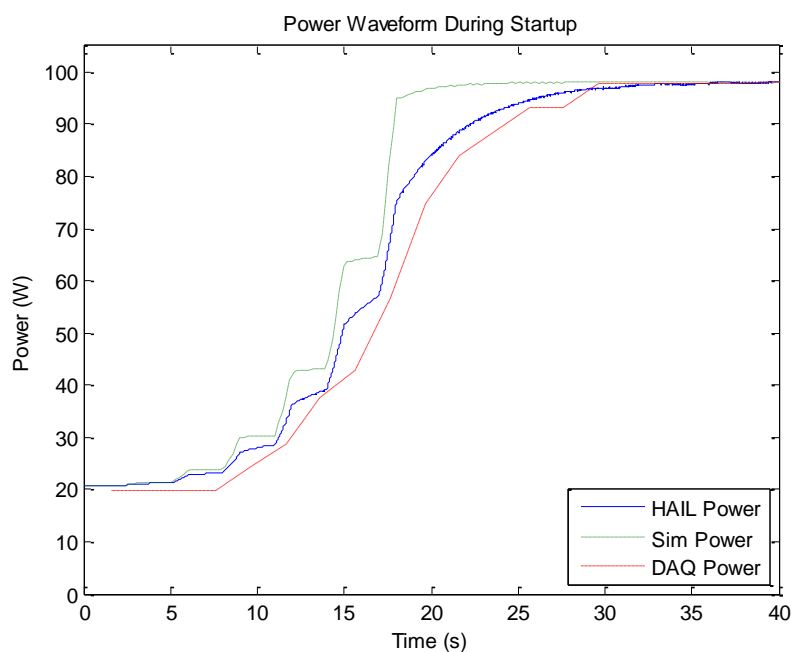


Figure 4.5: Total vehicle power consumption during startup of 3-knot 12-hour LWV trial

The error present in the dc load's interpretation of the current commands can clearly be seen in a plot of the commanded current waveform during the entire 12-hour run, as seen in Figure 4.6. Once the initial startup phase of the cycle is complete, the load settles into the closest discrete current step available. The load's current regulation can clearly be seen in the plot, due in large part to the fact that the scale of the Figure is on the order of mA steps. Once the current command crosses another discrete threshold, the load brings its current draw up to the new value, and continues in a well regulated fashion. These discrete steps introduce the largest portion of the error seen in the HAIL results, especially at very low current draw.

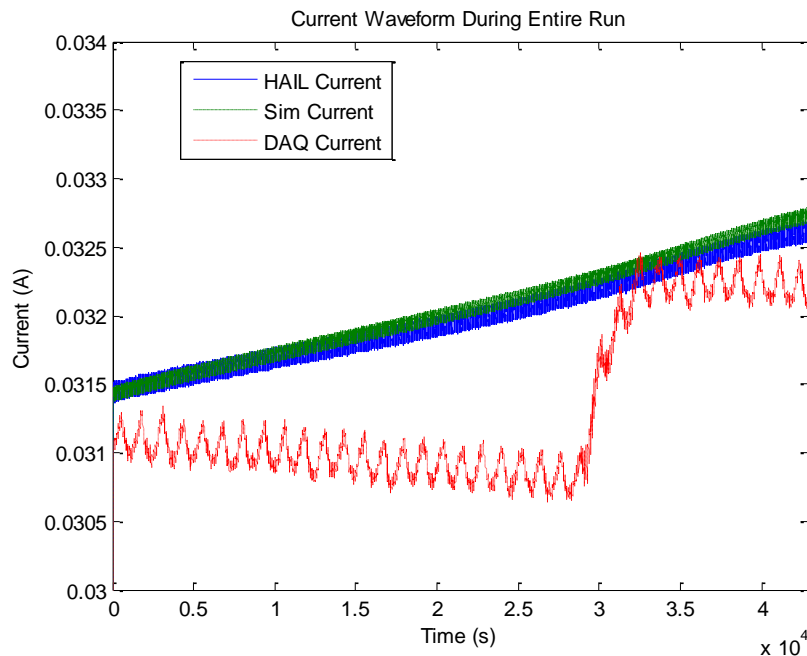


Figure 4.6: Waveform of current withdrawn from pack during 3-knot 12-hour LWV trial

In contrast to current, the voltage measurements taken by the HAIL platform match the externally recorded voltage levels quite well. The dc load's voltage measurement system, which provides the voltage feedback, has a much smaller error than the current level the load can maintain, coming in at $\pm 0.25\% \pm 40 \text{ mV}$ [20]. As the battery pack operates in the 20.09-

18.50 V range during the course of the various trials, the worst case error at 20.09 V would be approximately 0.0902 V, or 0.45%, a tenfold reduction from the error levels seen with the current command interpretation of the dc load. Figure 4.7 shows a close-up view of the voltage waveform shortly after the beginning of a 12-hour cycle. The voltage signal captured by the HAIL's A/D and the DAQ's measured voltage fall very close to the simulated voltage data.

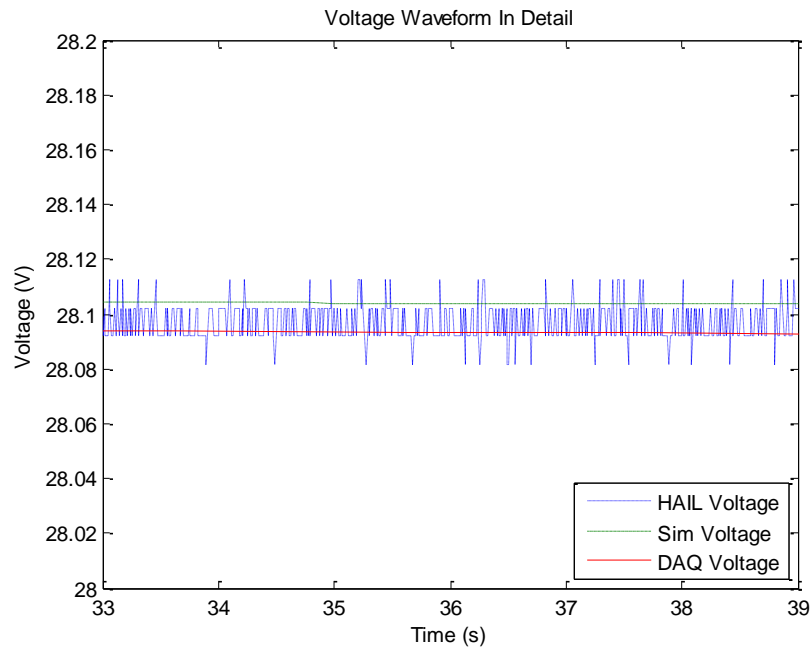


Figure 4.7: Close-up view of voltage waveforms during 3-knot 12-hour LWV trial

4.3.2 Light-weight vehicle, 5 knots, 6 hours

When the vehicle speed is increased to 5 knots, the requisite power to propel the vehicle through the water increases substantially. This increases the current draw as well, as the voltage level remains unchanged. As a result, the dc load is commanded to withdraw greater amounts of current, and the change in current commanded is faster than in the 3 knot case. These situations combine to result in an improved current profile, as seen in Figure 4.8. Because the

current draw changes faster during a shorter time frame, the discrete steps of the current load occur more frequently, and the resulting curve better approximates the current command.

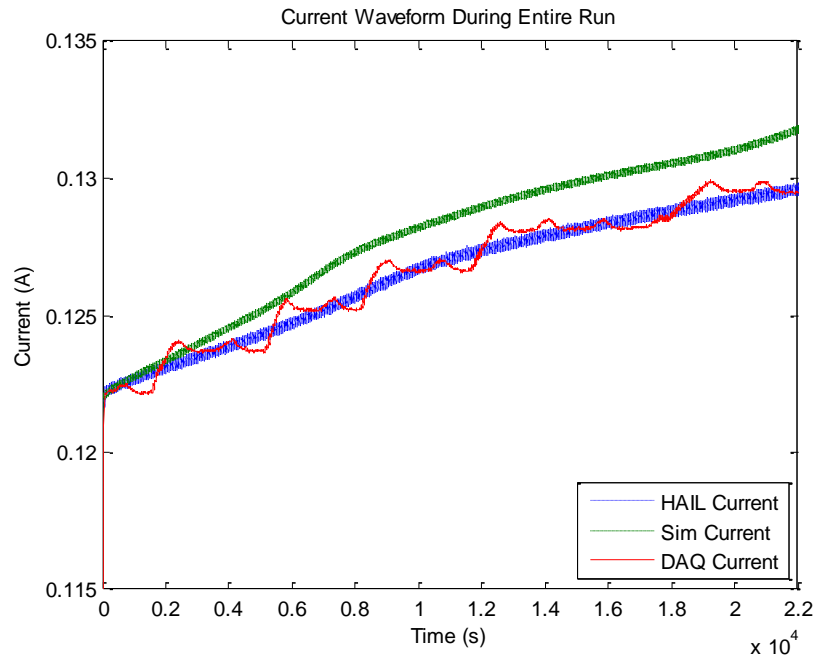


Figure 4.8: Close-up view of current waveforms during a 5-knot 6-hour LWV trial

The increased fidelity of the current source waveform when compared to the commands is reflected in the five trial runs. Table 4.5 lists the energy consumption and error figures for each run, and the mean error values fall to just above 1%. The first trial presents the only real deviation from the rest of the data set, and, based on the initial calibration numbers and the data plots, it appears to be a case of greater than average error in the dc load's interpretation of the current commands.

Table 4.5: Energy consumed and errors observed for 5-knot LWV runs

	HAIL Energy	DAQ Energy	Sim Energy	HAIL-DAQ Error	HAIL-Sim Error	DAQ-Sim Error
Trial 1	2402.7 W-hr	2353.4 W-hr	2401.9 W-hr	2.0499%	0.0329%	2.0177%
Trial 2	2402.3 W-hr	2379.4 W-hr	-	0.9519%	0.0168%	0.9352%
Trial 3	2402.3 W-hr	2379.7 W-hr	-	0.9377%	0.0161%	0.9217%
Trial 4	2402.3 W-hr	2383.9 W-hr	-	0.7647%	0.0178%	0.7470%
Trial 5	2402.3 W-hr	2385.4 W-hr	-	0.7035%	0.0172%	0.6864%
Mean				1.0815%	0.0202%	1.0616%

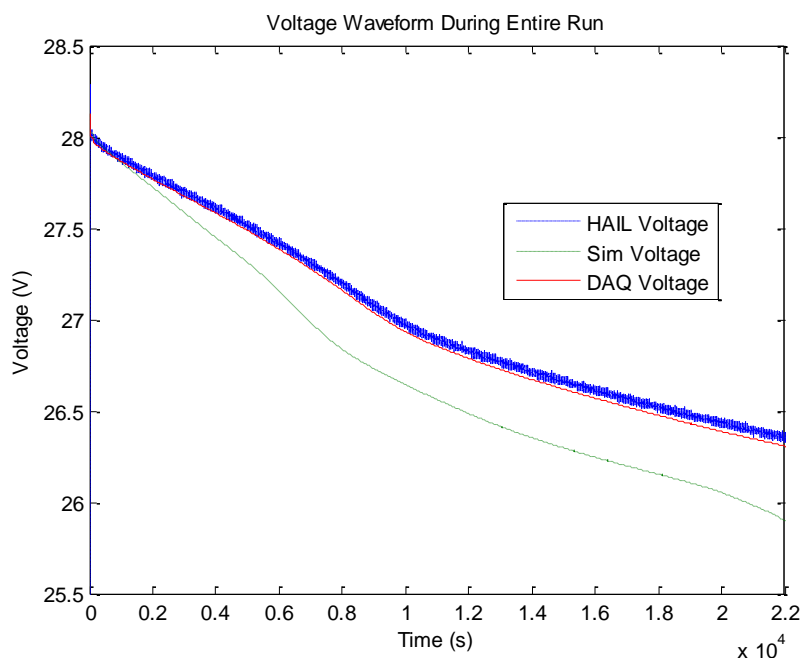


Figure 4.9: Close-up view of voltage waveforms during a 5-knot 6-hour LWV trial

However, even though the energy withdrawn from the batteries very closely matches the simulated result, there is a clear divergence in the experimental waveforms and the simulated one. The voltage waveform, seen in Figure 4.9, displays a similar divergence, which is to be expected given the close results in the energy calculations. The most likely reason for this deviation is the ripple seen in the current withdrawn from the battery pack. When the current drops, the terminal voltage rises due to a decreased discharge rate, meaning the simulation

needs to command slightly less power to maintain the correct power output. As the ripple continues its swing above and below the commanded value, this process repeats, and the deviation, slight at first, becomes more pronounced, leading in the end to a difference at the battery terminals of nearly 0.5 V. The battery model itself is most likely not the source of the error, given that the results for the previous set of 3-knot trials show no such aberration in the voltage waveform. The ripple in the 3-knot case was also less, further reducing the likelihood of a faulty model.

4.3.3 Man-portable vehicle, 3 knots, 12 hours

The second vehicle class to be examined, the man-portable size, is, in principle, a shrunken version of the light-weight vehicle examined above, with reduced diameter and energy storage. At 3 knots, the vehicle consumes approximately 47 W, as seen above, and as a result it will be capable of travelling for significant time spans without requiring a recharge. The five trials of the 3-knot speed profile resulted in the data in Table 4.6. Of note is the error between the three sets of data, with neither the DAQ nor HAIL data exceeding 1% error in relation to the simulation's results. The first trial run, in particular, displayed a very small error, coming in at less than 0.1%.

Table 4.6: Energy consumed and errors observed for 3-knot MP runs

	HAIL Energy	DAQ Energy	Sim Energy	HAIL- DAQ Error	HAIL- Sim Error	DAQ- Sim Error
Trial 1	565.02 W-hr	565.50 W-hr	565.04 W-hr	0.0843%	0.0031%	0.0812%
Trial 2	565.05 W-hr	559.70 W-hr	-	0.9470%	0.0011%	0.9459%
Trial 3	565.05 W-hr	560.65 W-hr	-	0.7790%	0.0019%	0.7771%
Trial 4	565.05 W-hr	560.29 W-hr	-	0.8419%	0.0011%	0.8408%
Trial 5	565.04 W-hr	559.05 W-hr	-	1.0598%	0.0005%	1.0594%
Mean				0.7424%	0.0015%	0.7409%

The plot of the current waveform in Figure 4.10 shows the now familiar effect of the limits of the dc load's resolution. The stepping of the current over the course of the simulated journey remains the most likely reason for the differences observed in Table 4.6. The variation between the HAIL's current commands and the simulated ideal case is minute, with the small error seen attributable to the error in the battery pack voltage reading the HAIL platform receives from the dc load. The variation in the HAIL's calculated power consumption is very small as well, providing another verification of the ability of the simulation to successfully track a velocity command and onboard loads over the course of 12 hours.

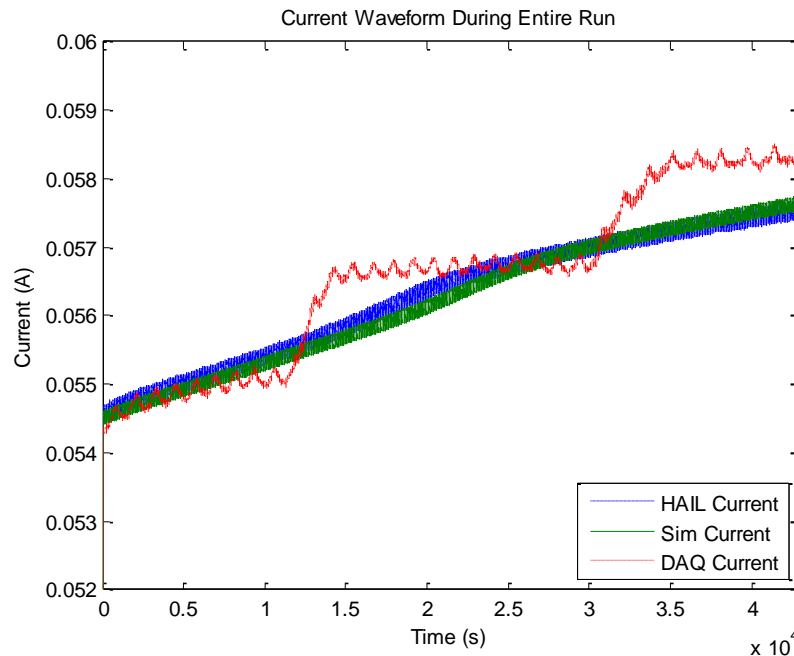


Figure 4.10: Close-up view of current waveforms during a 3-knot 12-hour MP trial

The voltage waveform plot in Figure 4.11 confirms the slight difference observed above, showing a deviation of the simulated voltage and actual voltage for a portion of the trial. The lower voltage would increase the current commanded, in order to keep the power constant.

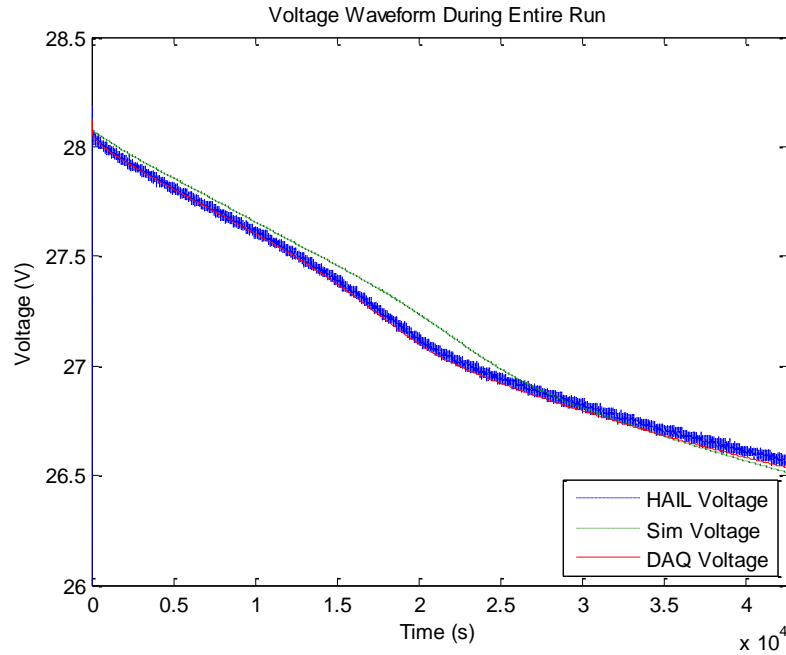


Figure 4.11: Complete view of voltage waveforms during a 3-knot 12-hour MP trial

The power waveform plot follows the same pattern, showing almost no deviation between the HAIL platform's internal power calculations and the numbers gathered during the simulated trial. Figure 4.12 shows an up-close view of the power waveform, and the simulated power waveform is indistinguishable from the noisier HAIL power signal; the two overlap each other exactly as they should. The DAQ power shows a slight error. It is attributable to the fact that the voltage reading on which the HAIL calculation depends has an uncertainty due to the measurement error described earlier.

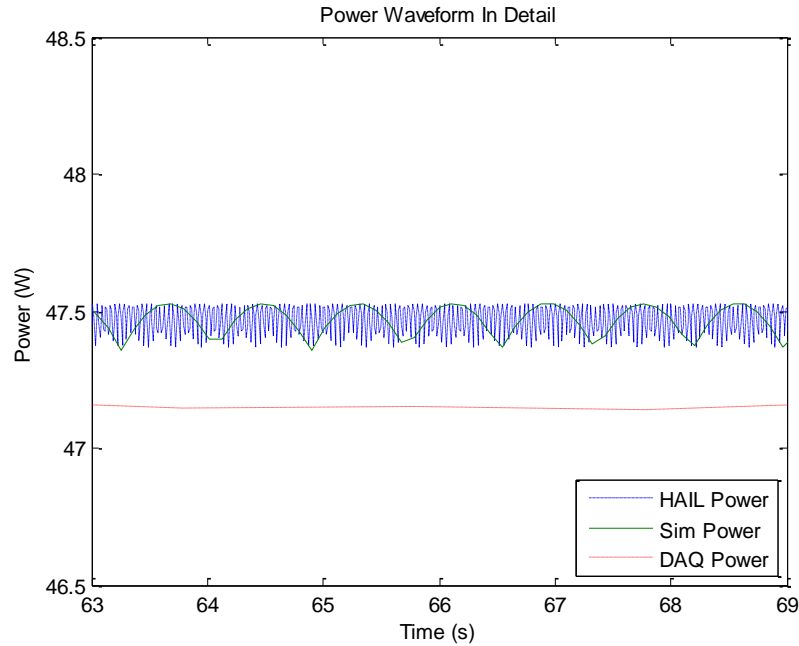


Figure 4.12: Close-up view of power waveforms during a 3-knot 12-hour MP trial

4.3.4 Man-portable vehicle, 5 knots, 6 hours

The final set of trials involves a 5-knot, 6-hour journey by the man-portable class vehicle. This is in essence the most stressful trial for the five cell battery pack being interfaced with the HAIL simulation. Although the overall power draw is far less for this case than for the light-weight vehicle's 5-knot 6-hour journey, the net current drain on each series arrangement of battery cells is highest. The current plot for the entire run in Figure 4.13 shows this clearly. The current command reaches a peak of nearly 180 mA at the end of the 6-hour run, nearly 50 mA more than the comparable 6-hour 5-knot journey the light-weight vehicle undertakes, as seen in Figure 4.8.

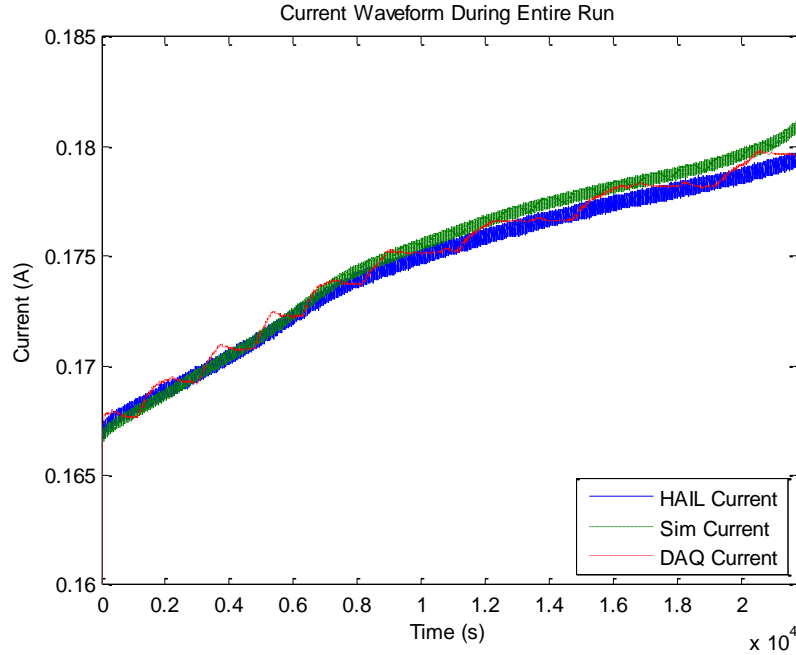


Figure 4.13: Close-up view of current waveforms during entire 5-knot 6-hour MP trial

The data gathered for energy consumed during the five trials is summarized in Table 4.7. Once again, the HAIL platform's internal power calculations and the simulated ideal are, for all intents and purposes, identical, with a mean error of 0.0095%. The HAIL platform and DAQ data mean error rate across the five trials is less than 1%, as is the DAQ data and simulated energy consumption error rate. As before, these numbers fall within the measurement and command response error of the dc load, rendering the slight existing error statistically irrelevant.

Table 4.7: Energy consumed and errors observed for 5-knot MP runs

	HAIL Energy	DAQ Energy	Sim Energy	HAIL-DAQ Error	HAIL-Sim Error	DAQ-Sim Error
Trial 1	879.33 W-hr	870.96 W-hr	879.25 W-hr	0.9481%	0.0093%	0.9389%
Trial 2	879.34 W-hr	870.58 W-hr	-	0.9961%	0.0103%	0.9859%
Trial 3	879.35 W-hr	870.78 W-hr	-	0.9753%	0.0118%	0.9637%
Trial 4	879.32 W-hr	870.94 W-hr	-	0.9527%	0.0077%	0.9451%
Trial 5	879.32 W-hr	871.48 W-hr		0.8918%	0.0082%	0.8836%
Mean				0.9528%	0.0095%	0.9434%

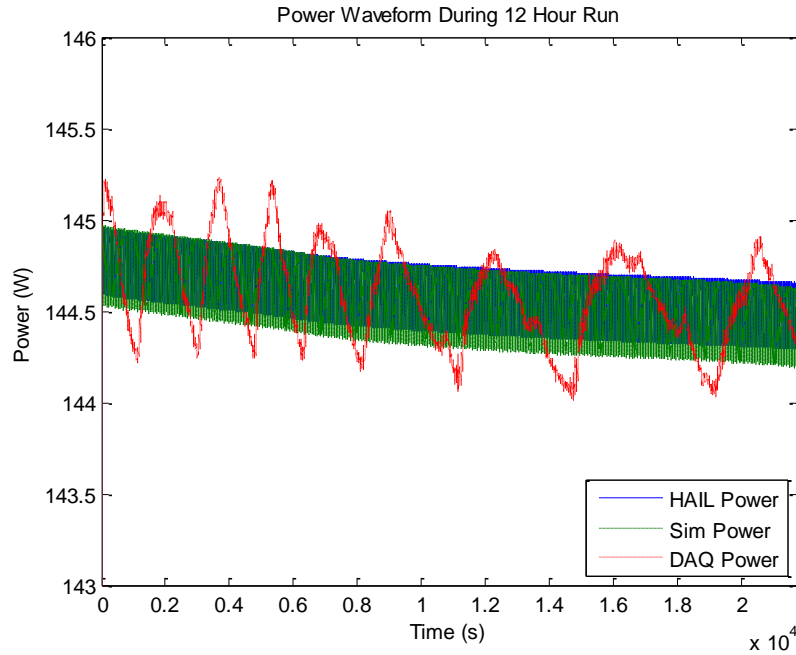


Figure 4.14: Close-up view of power waveforms during entire 5-knot 6-hour MP trial

The plot of the three power waveforms in Figure 4.14 shows a familiar image, with the HAIL's internally calculated power and the simulated power overlapping entirely, providing visual confirmation of the extremely small error rates in Table 4.7. The very low frequency ripple seen in the DAQ power waveform is further evidence of the dc load's discrete current-draw limitations, with each rising edge of the ripple corresponding to a step up in the load's current level. The corresponding drop is attributable to the decrease in terminal voltage that occurs as the battery pack discharges.

The voltage waveforms in Figure 4.15 observed by the HAIL platform and external DAQ exhibit the now familiar minimal error attributable to the dc load's measurement error in reporting the voltage level across the battery pack. The simulated pack's voltage shows the same increased rate of voltage droop as in the 5-knot 6-hour journey of the light-weight

vehicle. As in that case, the most likely source of this error between the two data sets can be the current ripple's effect on the terminal voltage. The simulator's current-load profile has virtually no low-frequency ripple, in contrast to the DAQ's observations. When the low-frequency current ripple exhibits a downward trend, the terminal voltage rises due to the resulting decrease in the voltage drop across the battery pack's internal impedance. This rising voltage prompts the HAIL platform to in turn command a lower current in order to maintain the desired power level. This effect is cumulative, increasing the deviation in the predicted and actual voltage with each rise and fall of the current load.

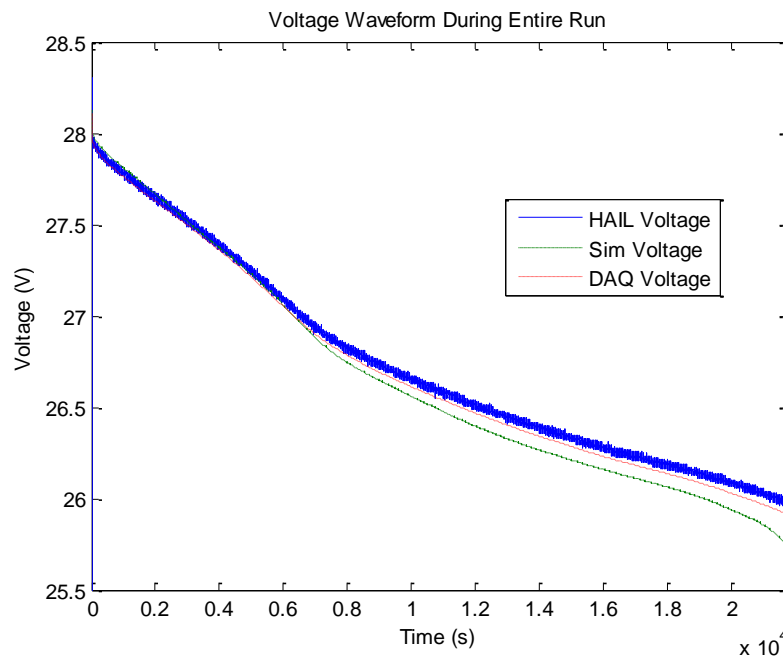


Figure 4.15: Complete view of voltage waveforms during entire 5-knot 6-hour MP trial

5. CONCLUSIONS

The ability of the HAIL platform to successfully track a simulated power demand profile has been verified using two separate vehicle types – the hybrid electric vehicle and the unmanned underwater vehicle. The HEV served as the proof of concept. Its verified ability to accurately track real-world behavior allowed the work to be focused on the xPC simulation platform and hardware interfaces, not the HEV simulation itself. Once the basic aspects of the hardware architecture were developed and tested, the implementation of this platform with a new and different dynamic system provided confirmation that it was indeed working as intended. The UUV model is a combination of the proven lithium-ion battery model and a new electric drive train, providing the basis for this model to be adapted to the HAIL environment. Although the UUV model's behavior is not directly compared to a matching real-world UUV, the verified battery model and commonly accepted drive train modeling allow the comparisons to remain valid.

The error seen in the original HEV implementation was due to the use of an insufficiently fast interface between the hardware and the simulation. With the implementation of an analog interface intended to send the current commands and monitor the pack voltage, the error was reduced significantly and the behavior of the HAIL bench-top platform matched that of the original simulation. With average error rates at less than 2% across all four UUV trial sets, the error rates observed fall within the measurement error present at the analog/digital interface of the HAIL platform. The combination of the dc load's $\pm 4.5\%$ current command interpretation error, discrete current load-stepping limitations, and a nearly 0.5% voltage readback error make the error observed in the results statistically insignificant.

6. FUTURE WORK

The HAIL platform has been validated in combination with a scaled down energy storage system and the associated hardware needed to control the charge/discharge rate. With the storage system complete, and seven of eight analog input/output pairs remaining free, the integration of additional hardware becomes the next challenge. The traction system presents one possible set of components that could be reproduced in a scaled down fashion in the lab, using an inverter and dynamometer to drive and load the electric machine being tested. This would allow for the evaluation of several different subsystems individually, and could provide insight into the combined behavior of all the components as an electric propulsion system responding to the commands issued by the real-time simulation linking them together.

The limited run-time problem remains, although the solution has already been conceptualized. If a 64-bit capable version of xPC becomes available, the solution is an upgrade to the newest version. If no such upgrade is available, another method to circumvent this would be to implement a supervisory program charged with overseeing the HAIL platform's operation. With either method the 13 hour barrier would be overcome, allowing real-time hardware evaluation for extended periods of time.

Outside of the realm of propulsion systems, the verified success of the HAIL platform's ability to reproduce a commanded behavior of a complex dynamic system in real time opens the door to a range of possibilities. A parallel arrangement of dc/dc converters could be implemented in the simulation environment and programmed to react to an externally connected set of controllers that regulate the behavior of each converter to a desired operating point. Or the opposite track could be taken, with the controller remaining in a simulated real-time

environment while the actual power conversion hardware is interfaced to the platform, relaying voltage and current levels back to the computer and accepting switching commands. The possibilities are limited only by the number of available I/O's and the computer's processing power, both of which can be expanded. The fundamentals of the HAIL platform remain the same, and will carry over to more or less powerful computational platforms, providing the option of multiple computers interfaced to each other and to hardware, each executing a portion of a much larger dynamic system.

REFERENCES

- [1] J. M. Timmermans, J. Van Mierlo, P. Lataire, F. Van Mulders, and Z. McCaffree, "Test platform for hybrid electric power systems: development of a HIL test platform," in *2007 European Conference on Power Electronics and Applications*, Aalborg, Denmark, 2-5 September, 2007, pp. 1-7.
- [2] L. Verhoeff, D. J. Verburg, H. A. Lupker, and L. J. J. Kusters, "VEHIL: A full-scale test methodology for intelligent transport systems, vehicles and subsystems," in *Proceedings of the IEEE Intelligent Vehicles Symposium 2000*, Dearborn, MI, October 3-5, 2000, pp. 369-375.
- [3] K. B. Wipke, M. R. Cuddy, and S. D. Burch, "ADVISOR 2.1: A user friendly advanced powertrain simulation using a combined forward/backward approach," *IEEE Transactions on Vehicular Technology*, vol. 48, no. 6, pp. 1751-1761, November 1999.
- [4] Z. Bin, F. Pin, and X. Guoqing, "Simulation of hybrid electric truck and plug-in hybrid electric truck based on ADVISOR," in *2007 IEEE International Conference on Integration Technology*, Shenzhen, China, March 20-24, 2007, pp. 455-458.
- [5] J. Huo and X. Guo, "Modeling and simulation of hybrid electric vehicles using HEVSIM and ADVISOR," in *2008 IEEE Vehicle Power and Propulsion Conference*, Harbin, China, September 3-5, 2008, pp. 1-5.
- [6] K. Athanasas and I. Dear, "Validation of complex vehicle systems of prototype vehicles," *IEEE Transactions on Vehicular Technology*, vol. 53, no. 6, pp. 1835-1846, November 2004.
- [7] A. Monti, S. D'Arco, and A. Deshmukh, "A new architecture for low cost power hardware in the loop testing of power electronics equipments," in *IEEE International Symposium on Industrial Electronics*, Cambridge, United Kingdom, June 20 – July 2, 2008, pp. 2183-2188.
- [8] P. Ridao, E. Batlle, D. Ribas, and M. Carreras, "NEPTUNE: A HIL simulator for multiple UUVs," in *OCEANS '04. MTS/IEEE TECHNO-OCEAN '04*, vol.1, pp. 524-531, 9-12 November 2004.

- [9] M. A. Kelf, "Hardware-in-the-loop simulation for undersea vehicle applications," in *Proceedings of the SPIE - The International Society for Optical Engineering*, vol. 4366, 2001, pp. 1-12.
- [10] B. C. Davis, P. Patron, and D. M. Lane, "An augmented reality architecture for the creation of hardware-in-the-loop & hybrid simulation test scenarios for unmanned underwater vehicles," in *OCEANS 2007*, September 29, 2007-Oct. 4, 2007, pp. 1-6.
- [11] J. G. Kassakian, N. K. Medora, and B. R. Rhodes, "Parity simulation of static power conversion systems," in *IEEE Power Electronics Specialists Conference*, 1977, pp. 324-328.
- [12] P. T. Krein and R. K. Baphna, "A microprocessor-based switching power converter test bed," in *22nd Annual IEEE Power Electronics Specialists Conference, 1991, PESC '91 Record*, 24-27 June, 1991, pp. 861-866.
- [13] D. L. Logue and P. T. Krein, "Dynamic hybrid vehicle simulation, version 1.0," University of Illinois, Urbana, IL, Technical Report UILU-ENG-98-0409, December 1998.
- [14] P. T. Krein and M. Amrhein, "Vehicle system and subsystem interactions with power electronics," University of Illinois, Urbana, IL, Technical Report UILU-ENG-2004-2505, July 2004.
- [15] M. Amrhein and P. T. Krein, "Dynamic simulation for analysis of hybrid electric vehicle system and subsystem interactions, including power electronics," *IEEE Trans. Vehicular Tech.*, vol. 54, no. 3, pp. 825-836, May 2005.
- [16] Information on Mathworks' xPC Target real time simulation platform can be found at: www.mathworks.com/products/xpctarget/
- [17] Panasonic CGR18560A Datasheet, Available: <http://industrial.panasonic.com/www-cgi/jvcr13pz.cgi?E+BA+3+ACA4001+CGR18650A+7+WW>
- [18] R. C. Kroeze and P. T. Krein, "Electrical battery model for use in dynamic electric vehicle simulations," in *Proceedings of PESC '08 – 39th IEEE Annual Power Electronics Specialists Conference*, June 15-19, 2008, pp. 1336-1342.
- [19] Information on MATLAB's memory limitations can be found at: <http://www.mathworks.com/support/tech-notes/1100/1110.html>

- [20] P. T. Krein, T. G. Roethemeyer, R. A. White, and B. R. Masterson, "Packaging and performance of an IGBT-based hybrid electric vehicle," in *Proceedings of the Power Electronics in Transportation, 1994*, 20-21 October, 1994, pp. 47-52.
- [21] Information on the Federal Urban Driving Schedule (FUDS) can be found at: <http://www.epa.gov/nvfel/testing/dynamometer.htm>
- [22] M. J. Tavernini, B. A. Niemoeller, and P. T. Krein, "Real-time low-level simulation of hybrid vehicle systems for hardware-in-the-loop applications," in *IEEE Vehicle Power and Propulsion Conference, 2009, VPPC '09*, 7-10 September, 2009, pp. 890-895.
- [23] *IEEE Standard Digital Interface for Programmable Instrumentation*, ANSI/IEEE Standard 488.1-1987, 1987-88, pp. 85-86.
- [24] *Characteristics of 28 Volt DC Electrical Systems in Military Vehicles*, MIL-STD-1275D, United States Department of Defense, August, 2006.
- [25] P. C. Krause, O. Wasnynczuk, and S. D. Sudhoff, *Analysis of Electric Machinery and Drive Systems*. Hoboken, NJ: Wiley-Interscience, 2002.
- [26] *Operating Manual: Agilent Technologies Single Input Electronic Load Family*, Agilent P/N 5951-2826, September 2004.

APPENDIX A. UUV INITIALIZATION CODE

A.1 UUV Initialization Code, Light-Weight Vehicle

```
%UUV Light Weight Vehicle initialization file
%Marco J. Tavernini, October 2009

P_controls=20; %power consumed by system control

%Sample times
T_sample=12e-6; %Sampling time
T_quanser_sample = round(.001/T_sample)*T_sample; % ~1ms

%scope decimation rates
Slower_decimation = round(0.01/T_sample);
Faster_decimation = round(0.0005/T_sample);

%Battery pack system

Battery_number=7; %Number of batteries in the pack, state 1
Batt_num_par=111;
Battery_number2=14; %Number of batteries in the pack, state 2
Batt_num_par2=44;
Initial_SOC=0.85;
SOC_threshold=0.2;
Init_term_voltage=4.018198;
Q_bat_max=7232.36; %Maximum pack energy in J

% HIL sim parameters

V_batt_undervolt = 15; %undervolt protection threshold, 3V per cell
V_batt_overnvoltage = 21; %overnvoltage protection threshold, 4.2V per cell

I_dc_supply = 3.0; %set Kenwood DC supply to output this current
I_prm_trim = 0; %Applies a dc offset to ext prgm signal sent to dc load

fprintf('Set Kenwood dc supply to %1.2f A current.\n',I_dc_supply + 0.13)

% i_dc_load_cmd_quantization_intv = 0.02; %force dc load to be set in steps
of 20mA
I_dc_cmd_upperlimit = 2*I_dc_supply; %max load current that can be commanded
if I_dc_cmd_upperlimit > 6
    I_dc_cmd_upperlimit = 60;
else
    I_dc_cmd_upperlimit = 6;
end
Cells_in_pack = 5; %number of cells in the battery pack under test

%HIL GPIB device parameters
```

```

dc_load_addr = 1;
T_gpib_device_sample = round(.25/T_sample)*T_sample; %about .3 secs
HIL_gpib_commands; %load gpib command structs
fprintf('HIL GPIB Device Parameters Set.\n')

% Analog battery interface parameters
Icmd2Vprgm_gain = 10/I_dc_cmd_upperlimit*1/1.012; %second term trims Vprgm
input
Vmon2Vpack_gain = 60/10*19.55/19.3742; %second term needed to trim Vmon
input

%Propeller torque speed relationship
%Speed vs. shaft torque map is created

IM_fan_omega=[0;52.36;104.72;157.08;188.50;209.44;261.80;314.16;366.52;...
376.99;418.88;471.24;523.60;565.49;575.96;628.32;680.68;733.04];
IM_fan_torque=[0;0.363;0.561;0.603;0.614;0.621;0.683;0.868;0.950;0.992;...
1.134;1.269;1.460;1.700;1.750;2.044;2.262;2.618];

%Electronic drive

R_IGBT=2.2e-3; %IGBT on resistance
V_IGBT=1; %IGBT forward voltage drop

%Setup Vehicle dynamics
init_veh_speed=0;
Va = 0; %ambient fluid velocity (m/s)
fan_area = 0.0163; %propeller surface area (m^2)
prop_radius = 0.05; %propeller radius (m)
%Grade=0; %Road grade
Rho=1000; %water density (kg/m^3)
C_drag=0.3; %Vehicle drag coefficient
frontal_area=0.0823; %Vehicle frontal area (m^2)
grav_const=9.81; %m/s^2
Total_mass=240; %Total vehicle mass (kg)
M_effective=240; %kg (unsure of moment of inertia of tires)
G = 1; %motor to prop gear ratio
FG = 100;

%%%%%%%%%%%% On board system parameters %%%%%%%%%%%%%%

active_p = 50; %active sonar power draw
passive_p = 10; %passive sonar power draw
gps_p = 10; %Comm/GPS power draw
floor_p = 25; %floor mapping power draw
water_p = 10; %ocean characterization power draw
payload_p = 40; %payload deployment power draw

%%%%%%%%%%%% DC Motor parameters %%%%%%%%%%%%%%

```

```
%torque controller
V_dcmax = 28; %maximum rated voltage of motor
T_dcmax = 3; %maximum rated torque of motor

%Machine parameters

Ld = 0.0114;
Lq = 0.0114;
Bm = 0.000;
P = 40;

rs = 2.98;
flux = 0.156;

J = 0.000179;

%Current Controller parameters
CR_gain=50; %Current regulator gain
IM_CL=50; %current limit placed on switching devices
```


A.2 UUV Initialization Code, Man-Portable Vehicle

```
%UUV Man portable initialization file
%Marco J. Tavernini, October 2009

P_controls=20; %power consumed by system control

%Sample times
T_sample=11e-6; %Sampling time
T_quanser_sample = round(.001/T_sample)*T_sample; % ~1ms

%scope decimation rates
Slower_decimation = round(0.01/T_sample);
Faster_decimation = round(0.0005/T_sample);

%Battery pack system

Battery_number=7; %Number of batteries in the pack, state 1
Batt_num_par=31;
Battery_number2=12; %Number of batteries in the pack, state 2
Batt_num_par2=14;
Initial_SOC=0.85;
SOC_threshold=0.2;
Init_term_voltage=4.018198;
Q_bat_max=7232.36; %Maximum pack energy in J

% HIL sim parameters

V_batt_undervolt = 15; %undervolt protection threshold, 3V per cell
V_batt_overnvoltage = 21; %overnvoltage protection threshold, 4.2V per cell

I_dc_supply = 3.0; %set Kenwood DC supply to output this current
I_prm_trim = 0; %Applies a dc offset to ext prgm signal sent to dc load

fprintf('Set Kenwood dc supply to %1.2f A current.\n',I_dc_supply + 0.13)

% i_dc_load_cmd_quantization_intv = 0.02; %force dc load to be set in steps
of 20mA
I_dc_cmd_upperlimit = 2*I_dc_supply; %max load current that can be commanded
if I_dc_cmd_upperlimit > 6
    I_dc_cmd_upperlimit = 60;
else
    I_dc_cmd_upperlimit = 6;
end
Cells_in_pack = 5; %number of cells in the battery pack under test

%HIL GPIB device parameters
dc_load_addr = 1;
T_gpiib_device_sample = round(.25/T_sample)*T_sample; %about .3 secs
HIL_gpiib_commands; %load gpiib command structs
```

```

fprintf('HIL GPIB Device Parameters Set.\n')

% Analog battery interface parameters
Icmd2Vprgm_gain = 10/I_dc_cmd_upperlimit*1/1.012; %second term trims Vprgm
input
Vmon2Vpack_gain = 60/10*19.55/19.3742; %second term needed to trim Vmon
input

clear temp;
clear temp_inv;

%Propeller torque speed relationship
%Speed vs. shaft torque map is created

IM_fan_omega=[0;52.36;104.72;157.08;188.50;209.44;261.80;314.16;366.52;...
              376.99;418.88;471.24;523.60;565.49;575.96;628.32;680.68;733.04];
IM_fan_torque=[0;0.363;0.561;0.603;0.614;0.621;0.683;0.868;0.950;0.992;...
              1.134;1.269;1.460;1.700;1.750;2.044;2.262;2.618];

%Electronic drive

R_IGBT=2.2e-3; %IGBT on resistance
V_IGBT=1; %IGBT forward voltage drop

%Setup Vehicle dynamics
init_veh_speed=0;
Va = 0; %ambient fluid velocity (m/s)
fan_area = 0.002; %propeller surface area (m^2)
prop_radius = 0.025; %propeller radius (m)
%Grade=0; %Road grade
Rho=1000; %water density (kg/m^3)
C_drag=0.3; %Vehicle drag coefficient
frontal_area=0.0285; %Vehicle frontal area (m^2)
grav_const=9.81; %m/s^2
Total_mass=45; %Total vehicle mass (kg)
M_effective=45; %kg (unsure of moment of inertia of tires)
G = 0.1; %motor to prop gear ratio
FG = 100;

%%%%%%%%%%%% On board system parameters %%%%%%%%%%%%%

active_p = 50;      %active sonar power draw
passive_p = 10;     %passive sonar power draw
gps_p = 10;         %Comm/GPS power draw
floor_p = 25;       %floor mapping power draw
water_p = 10;       %ocean characterization power draw
payload_p = 40;     %payload deployment power draw

%%%%%%%%%%%% DC Motor parameters %%%%%%%%%%%%%

%torque controller

```

```

V_dcmax = 28; %maximum rated voltage of motor
T_dcmax = 3; %maximum rated torque of motor

%Machine parameters

Ld = 0.0114;
Lq = 0.0114;
Bm = 0.000;
P = 4;

rs = 2.98;
flux = 0.156;

J = 0.000179;

%Current Controller parameters
CR_gain=50; %Current regulator gain
IM_CL=50; %current limit placed on switching devices

```

APPENDIX B. VEHICLE TRIAL DATA

B.1 Light Weight Vehicle Trial Data

3 Knots, 12 Hours

Trial 1	@ DC Load	@ DAQ
Start VOC	20.09 V	20.086 V
Current	n/a	0.0001 A into pack
End VOC	19.32 V	19.325 V

Trial 2	@ DC Load	@ DAQ
Start VOC	20.09 V	20.0875 V
Current	n/a	0.0002 A into pack
End VOC	19.34 V	19.3416 V

Trial 3	@ DC Load	@ DAQ
Start VOC	20.09 V	20.0889 V
Current	n/a	0.0004 A into pack
End VOC	19.32 V	19.3304 V

Trial 4	@ DC Load	@ DAQ
Start VOC	20.09 V	20.082
Current	n/a	0.0006 A into pack
End VOC	19.32 V	19.3176 V

Trial 5	@ DC Load	@ DAQ
Start VOC	20.09 V	20.082 V
Current	n/a	0.0003 A into pack
End VOC	19.34 V	19.3328 V

5 Knots, 6 Hours

Trial 1	@ DC Load	@ DAQ
Start VOC	20.09 V	20.915 V
Current	n/a	0.00016 A into pack
End VOC	18.94 V	18.947 V

Trial 2	@ DC Load	@ DAQ
Start VOC	20.09 V	20.0816 V
Current	n/a	0.0018 A into pack
End VOC	18.96 V	18.9642 V

Trial 3	@ DC Load	@ DAQ
Start VOC	20.09 V	20.0888
Current	n/a	0.00045 A into pack
End VOC	18.93 V	18.9301 V

Trial 4	@ DC Load	@ DAQ
Start VOC	20.09 V	20.086 V
Current	n/a	0.00035 A into pack
End VOC	18.94 V	18.9325 V

Trial 5	@ DC Load	@ DAQ
Start VOC	20.09 V	20.09
Current	n/a	0.0006 A into pack
End VOC	18.925 V	18.93 V

B.2 Man Portable Vehicle Trial Data

3 Knots, 12 Hours

Trial 1	@ DC Load	@ DAQ
Start VOC	20.09 V	20.0875 V
Current	n/a	0.0001 A into pack
End VOC	19.01 V	19.015 V

Trial 2	@ DC Load	@ DAQ
Start VOC	20.09 V	20.088 V
Current	n/a	0.00012 A into pack
End VOC	19.04 V	19.0325 V

Trial 3	@ DC Load	@ DAQ
Start VOC	20.09 V	20.0878 V
Current	n/a	0.0003 A into pack
End VOC	19.04 V	19.0336 V

Trial 4	@ DC Load	@ DAQ
Start VOC	20.09 V	20.0838 V
Current	n/a	0.00045 A into pack
End VOC	19.04 V	19.0335 V

Trial 5	@ DC Load	@ DAQ
Start VOC	20.09 V	20.0825 V
Current	n/a	0.00077 A into pack
End VOC	19.04 V	19.0332 V

5 Knots, 6 Hours

Trial 1	@ DC Load	@ DAQ
Start VOC	20.09 V	20.0873 V
Current	n/a	0.0001 A into pack
End VOC	18.71 V	18.7157 V

Trial 2	@ DC Load	@ DAQ
Start VOC	20.09 V	20.0877 V
Current	n/a	0.0004 A into pack
End VOC	18.71 V	18.7145 V

Trial 3	@ DC Load	@ DAQ
Start VOC	20.09 V	20.0907 V
Current	n/a	0.0006 A into pack
End VOC	18.71 V	18.7169 V

Trial 4	@ DC Load	@ DAQ
Start VOC	20.09 V	20.0838 V
Current	n/a	0.0007 A into pack
End VOC	18.73 V	18.718 V

Trial 5	@ DC Load	@ DAQ
Start VOC	20.09 V	20.089 V
Current	n/a	0.0006 A into pack
End VOC	18.73 V	18.7204 V